

See discussions, stats, and author profiles for this publication at: <https://www.researchgate.net/publication/278229306>

Autonomous Control of Unmanned Combat Air Vehicles

Article *in* IEEE control systems · October 2012

CITATIONS

7

READS

243

2 authors:



Nazim Kemal Ure
Istanbul Technical University

54 PUBLICATIONS 596 CITATIONS

[SEE PROFILE](#)



Gokhan Inalhan
Istanbul Technical University

115 PUBLICATIONS 2,198 CITATIONS

[SEE PROFILE](#)

Some of the authors of this publication are also working on these related projects:



System Identification of a Fixed-Wing UAV [View project](#)



COPTRA: Combining Probable Trajectories [View project](#)

IEEE

control systems

MAGAZINE

OCTOBER 2012 VOLUME 32 NUMBER 5



Unmanned Aerial Vehicle Special Issue



Control Systems Society
Advancing Control Science
and Technology



N. KEMAL URE and
GOKHAN INALHAN

There is a growing demand for unmanned air vehicles (UAVs) with combat capabilities in battlefield scenarios [1]. Whether this capability is for evasive maneuvers or for flying attack patterns, unmanned combat air vehicles (UCAVs) are expected to operate in dense and often threatening environments that require aggressive trajectory planning and controls [1]. These trajectories often require the use of maneuvering capability over the full flight envelope of the aircraft. Examples of such trajectories are high-g turns and high angle-of-attack maneuvers. This article presents the development of a multimodal flight control and flight path planning scheme that allows the vehicle to autonomously perform agile maneuvers over its full flight envelope. The key element of this scheme is the maneuver decomposition methodology, which aims to reduce the complexity of the planning and control problems for UCAVs. This article demonstrates how a parameterized family of maneuver modes for a UCAV can be developed systematically and how



Autonomous Control of Unmanned Combat Air Vehicles

DESIGN OF A MULTIMODAL CONTROL AND FLIGHT PLANNING FRAMEWORK FOR AGILE MANEUVERING

Digital Object Identifier 10.1109/MCS.2012.2205532
Date of publication: 14 September 2012

This article presents the development of a multimodal flight control and flight path planning scheme that allows the vehicle to autonomously perform agile maneuvers over its full flight envelope.

an arbitrary agile maneuver can be decomposed into simpler segments. In addition, the article presents a multimodal flight control scheme in which each of the maneuver modes is controlled locally by a sliding mode controller. The overall capability of the system is demonstrated in challenging scenarios such as navigation in dense environments and autonomous execution of aerobatics competition sequences.

The ability of UCAVs to autonomously synthesize and execute agile maneuvers in complex and dynamic environments is an enabling technology for future air combat scenarios driven by performance and safety goals. The modeling and control of agile maneuvers has been investigated in both theoretical and experimental studies [2], [3]. In recent years, due to the complexity of six-degrees-of-freedom (6DOF) nonlinear aircraft dynamics, the general trend for modeling agile maneuvers has shifted toward decomposing the aircraft dynamics into a set of simplified predefined maneuvers. This concept is not uncommon to the motion planning community; indeed, motion description languages and quantized control concepts are adopted into motion planning [4] to reduce the complexity of the planning problems. Most of these languages are related to the concept of hybrid systems [5], which describes the motion of the vehicle by using discrete states and switching conditions. In this form, each discrete state has its own continuous dynamics, and the switches allow jumps between discrete states and dynamic models according to input and state conditions.

There has been a significant amount of research on motion planning for agile vehicles. The control of nonholonomic robotic systems based on languages that classify behaviors and reactions has been investigated [6]. Closed-loop hybrid control systems have been used for the control and path planning of mobile robots [7], [8]. For aerospace vehicles, a hybrid model for aircraft traffic management has been developed [9]. The hybrid system representation provides a means to 1) calculate reachable sets of the system and 2) design hybrid control laws to drive the system to safe states [10]. The description of aircraft dynamics as a hybrid system also has been studied for the control of both single and multiple aircraft [11], [12]. Motion planning for

agile vehicles using discrete maneuvers has been studied [13], which involves the development of a maneuver automaton that uses a collection of feasible system trajectories to represent the building blocks of the motion plan of the aircraft. Sequences of discrete maneuvers synthesized in this framework are tracked by using a nonlinear trajectory control system. Motion plans and controllable trajectories are restricted to the library of the aforementioned maneuver automaton. These libraries may be built by using interpolation between feasible trajectories [14]. This approach has been extended for the online planning of feasible trajectories in partially unknown environments by using receding horizon iterations [15]. A survey is available on planning and control methods based on discretization of robot motion [16] that contains information on the strengths and weaknesses of various approaches.

Another facet of the agile flight controls problem is the need for low-level feedback control systems that can execute maneuvers generated by the motion planners. Since linear control system tracking capabilities are limited to trimmed or nonaggressive trajectories, the application of nonlinear control theory to aircraft dynamics has been studied extensively. Two of the applicable nonlinear control techniques are feedback linearization [17], [18] and sliding mode control (SMC) [19]. Unfortunately, these techniques cannot be directly applied to the trajectory control of aircraft, as the controlled outputs render the internal dynamics of the aircraft unstable [20] in many cases. This class of controlled outputs are referred to as nonminimum-phase (NMP) outputs. Earlier works in this area (for example, [21] and [22]) neglect the effect of the NMP outputs on the control system design but show in simulations that their effect is negligible for the types of aircraft models that they considered. Backstepping controller design has been applied for the control of agile maneuvers for miniature helicopters that ensures bounded tracking error for NMP outputs [23]. An alternative way to overcome the NMP effect is to perform the stable inversion technique. This approach has been discussed for both conventional and vertical takeoff and landing aircraft models [24]–[26]. However, the stable inversion technique limits the full control bandwidth of the aircraft and diminishes the maneuvering capability needed to attain stability. On the other hand, sliding mode

controllers [20] offer robustness to a wide class of uncertainties, and the controllers can be integrated with a dynamic compensator to overcome the NMP effect (to a certain degree) on nonlinear aircraft control [27].

In addition to the theoretical developments and simulation studies, a substantial amount of experimental work has been conducted on the planning and control of agile aircraft. For instance, fast transitions have been demonstrated between hovering and level-flight positions for a fixed wing micro-aircraft flying indoors [28]. A control law has been designed for a specific aerobatic maneuver in which the control system fused a prior pilot-executed feed-forward commands with trajectory tracking feedback controller [29]. This controller was successfully demonstrated for a specific aerobatic trajectory by using an outside flying microhelicopter. Recently, machine learning techniques have been applied for the autonomous control of specific aerobatics maneuvers such as inverted flight [30]. This technique was also successfully demonstrated for a series of specific maneuvers and trajectories on a microhelicopter flying outdoors.

In this article, the treatment of agile flight hinges on the development of a multimodal flight control framework. The basic idea of the framework is to develop a family of parameterized maneuver sets that can be used to decompose an arbitrary flight path. This idea is inspired by maneuver sequences explained in aerobatics instruction books [31], [32], [33] and strategic maneuvers executed by fighter pilots [34]. These references indicate that most of the combat maneuvers are flown by combining sequences of elementary modes. This approach also simplifies the maneuver execution process. An aerobatic flight example which utilizes this sequencing process is illustrated in Figure 1.

The main advantage of this approach is the ability to treat the control and planning problems separately for each submaneuver. This separation results in a considerable complexity reduction during the design process. In the subsequent sections, we first present the modeling of agile maneuvers by using a set of maneuver modes and associated modal inputs that span the flight envelope of the aircraft. Later, a family of nonlinear feedback controllers is

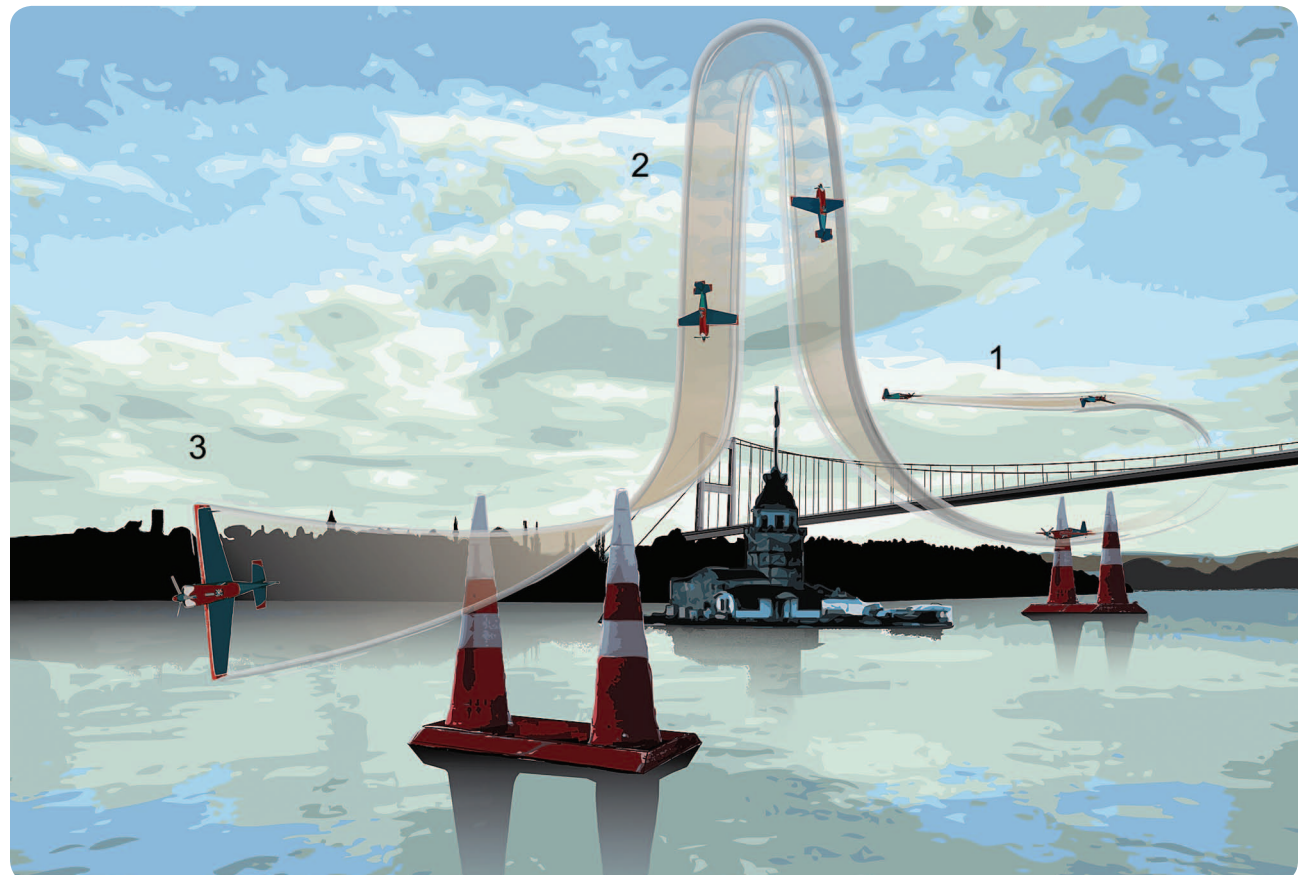


FIGURE 1 A maneuver sequence executed for an aerobatics competition. 1) The sequence starts with a split-S, a popular aerobatics maneuver, where the aircraft is inverted to enter the loop with head inside. 2) The sequence continues with a hammerhead, in which the aircraft climbs with 90° pitch angle relative to the ground and yaws to right at the top of the climb to change the direction of flight to a rapid descent. 3) The sequence ends with the aircraft back in level flight in a knife edge position, where the aircraft is completely banked to the left. Although the overall sequence is complex, it is seen that it can be decomposed into smaller segments.

Another facet of the agile flight controls problem is the need for low-level feedback control systems that can execute maneuvers generated by the motion planners.

presented for the autonomous execution of the selected maneuver modes. The final section presents two applications that utilize the modal control framework. The first application is the flight planning and control of a UCAV flying in a dense urban environment with obstacles. The second application is the flight control of an unmanned F-16 aircraft (with a high-fidelity nonlinear mathematical model) that executes an aerobatic air show exhibition flight sequence autonomously. Both of these applications demonstrate autonomous flight controls and agile maneuvering beyond the capabilities a human pilot and standard unmanned air vehicle flight controls.

MANEUVER DECOMPOSITION METHODOLOGY

This section provides details on the selection of maneuver modes and associated maneuver parameters by exploiting the existing knowledge on aerobatic flight and air combat. For a brief review of aerobatics and air combat maneuvers, see "Aerobatics and Air Combat Maneuvering." An in-depth inspection of agile maneuvers provides an intuitive insight into the design of the maneuver decomposition methodology. The main aim of the design process is to come up with a number of maneuver modes rich enough to capture full flight envelope dynamics, while keeping the number of modes small enough to simplify the controller and planner design process.

Selection of State-Space Variables and Mathematical Model

Aircraft dynamics in nonlinear state-space form is given by

$$\dot{x} = f(x, u), \quad x \in \mathbb{R}^n, \quad u \in \mathbb{R}^m, \quad (1)$$

where n is the number of states and m is the number of inputs. The position and the angular orientation of the aircraft constitute the basics of the states. Positional variables presented by the vector ρ are selected as a set of axes of a Cartesian coordinate system. Variables within these set of axes are denoted as $[n_p, e_p, h]^T$, which are north position, east position, and altitude, respectively. However, in some cases Cartesian coordinates may not be preferable since most of the previously mentioned agile maneuvers consist of circular trajectories. For this reason, we use two different cylindrical coordinate systems, namely, longitudinal cylindrical coordinates $[r_{lon}, \eta_{lon}, e_p]^T$ and lateral cylindrical coordinates $[r_{lat}, \eta_{lat}, h]^T$. Cylindrical

and Cartesian coordinate systems in inertial axes are displayed in Figure 2.

For velocity-related variables, a common choice is the trio $[V_T, \alpha, \beta]^T$ in which V_T is the total speed and α and β are angle of attack and sideslip angles. Aerodynamic angles α and β describe the relative rotation of the aircraft's velocity vector with respect to the body axes. An alternative approach is to use components of velocity vector in body axes as $[U, V, W]^T$. Another set of variables that is particularly useful for modeling cylindrical maneuvers is the Euler angles of the velocity vector with respect to inertial axes with $[\psi_w, \theta_w, \phi_w]^T$. The rotation sequence of pitch and yaw angles is going to be switched in certain places to simplify equations. These angles are referred as $[\psi'_w, \theta'_w, \phi'_w]^T$ throughout the article.

For orientation parameterization, Euler angles with respect to inertial axes, $[\psi, \theta, \phi]^T$, are used. These angles are also referred to as yaw, pitch, and roll angles, respectively. This formulation comes with potential numeric problems as the differential equations associated with Euler angle parameterization is known to be singular at 90° of pitch angle [35]. To overcome this difficulty, singularity-free quaternion parameterization given by quadruple $[\beta_0, \beta_1, \beta_2, \beta_3]^T$ can be considered. Because of the physical insight provided by Euler angles, we use the Euler angles

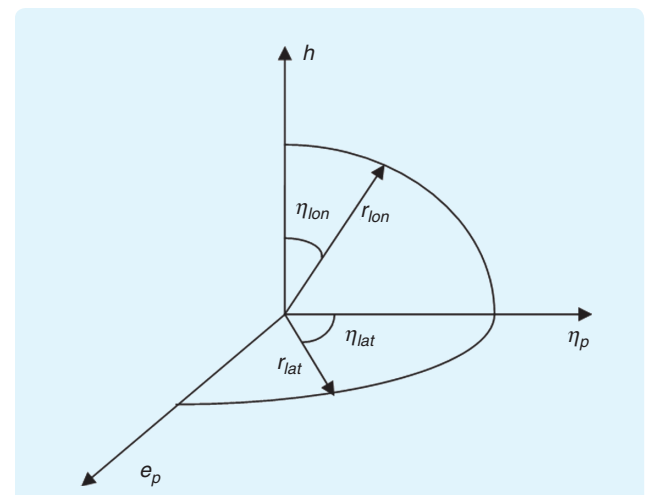


FIGURE 2 Cartesian and cylindrical coordinates. Cartesian coordinates are appropriate for modeling rectilinear paths such as level flight and climbs. On the other hand, cylindrical coordinates are more appropriate for modeling loops and 3D maneuvers.

Aerobatics and Air Combat Maneuvering

Aerobatics, which is a combination of the words *acrobatics* and *aeronautics*, is a popular form of entertainment where the aircraft is flown through unusual attitudes through a combination of circular trajectories (loops) and lines [31].

Although aerobatics is usually referred to as stunts performed by an airplane, most of the maneuvers are directly influenced by evasive maneuvers executed by fighter aircraft pilots. Since aerobatic flight spans a wide selection of the possible aircraft maneuvers and these maneuvers are usually performed at the edge of the flight envelope, it is of great interest to inspect the nature and the variety of aerobatic maneuvers for developing a maneuver library for a UCAV.

Some of the frequently performed aerobatics maneuvers that are encountered in both air shows and competitions are shown in Figures S1 and S2, in terms of path-attitude plots from top to the bottom. The hammerhead maneuver, which is also seen in Figure 1, is a combination of a sharp climb and descent with 180° of rotation on the yaw axis. The maneuver called the half Cuban eight combines a 3/4 loop with a slow roll and descent to reverse the direction of the aircraft without loss in the altitude.

Now let us consider the modular structure of the aerobatics. A quick inspection of Figures S1 and S2 indicates that aerobatic maneuvers can be categorized into two categories: elementary maneuvers and maneuvers that can be represented as combination of elementary maneuvers. For example, a hammerhead is a combination of climb/descent and yaw

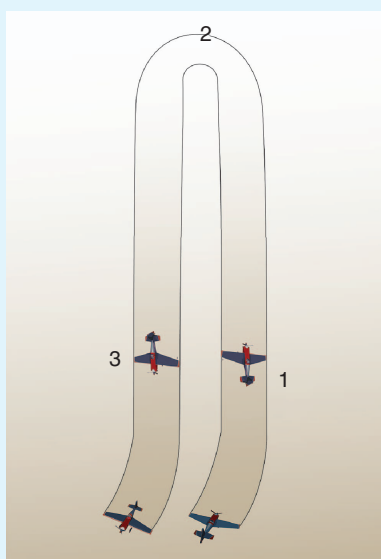


FIGURE S1 The hammerhead maneuver. 1) The aircraft starts to climb sharply and then performs a quick yaw rotation 2) to reverse the direction. 3) At the end of the maneuver, the aircraft recovers from descent to level flight.

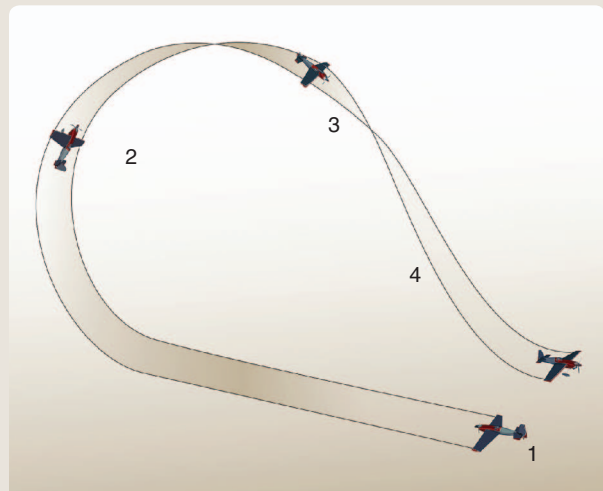


FIGURE S2 The half Cuban eight maneuver. 1) The aircraft starts in level flight and 2) draws a half loop in the longitudinal plane. At the top of the loop 3), the aircraft starts to descend on a straight path and rolls to 4) regulate back to level flight from descent.

rotation; similarly, a half Cuban eight can be represented as a combination of a loop, rotation on the roll axis, and descent. In fact, rolls and loops are accepted as building blocks of arbitrary aerobatic maneuvers [31]. This modular structure gives the pilot the flexibility of learning the basic maneuvers before flying more challenging maneuvers. However, mastering elementary maneuvers does not necessarily indicate that the pilot would fly combined maneuvers easily; passing from one maneuver to another is another subject that is strongly correlated with the limits of the aircraft as well as the associated transition logic.

Various books on aerobatics [31], [33] illustrate the techniques on flying elementary and combined maneuvers. Basically, there are two significant aspects of flying aerobatic maneuvers: 1) entering the maneuver with appropriate speed and orientation and 2) keeping the aircraft in limits of the flight envelope while avoiding stalling and spinning and keeping track of the maneuver parameters such as altitude and roll rate. These aspects are also important during switching between maneuvers. Looking at the composite flight trajectory from a mode-based point of view, each mode possesses an ideal initial condition and flying objective to fly correctly and safely. Once the transition logic between each mode is implemented, it may be possible to derive a switched control logic that operates on elementary flight modes to fly arbitrary complex aerobatics maneuvers.

Air combat maneuvering (ACM) is a class of maneuvers performed by a fighter aircraft in either a defensive or aggressive manner to gain tactical advantage over enemy aircraft during air combat. These maneuvers are usually more complex than aerobatic maneuvers and evolve in three dimensions

as ACM maneuvers are not motivated by artistic quality but to evade or attack the target aircraft. One of the main aims of air combat is to achieve a position within a specific area at the rear of the target, referred to as the *cone of vulnerability*. Once this aim is achieved, the pursuer pilot can fire the aircraft's guns to bring the target down. More information on air combat maneuvering and tactics is available [34].

A large portion of aerobatics shares maneuvers with ACM, since most of the aerobatics maneuvers are derived from maneuvers invented by fighter aircraft pilots. Two combat maneuvers for one-on-one air combat are provided in Figures S3 and S4, respectively. These maneuvers are known as *high yo-yo* and *split-S* maneuvers.

High yo-yo shows how a defender aircraft can turn the situation to its own advantage by executing an out-of-plane maneuver. The initial position attacker is behind the defender's

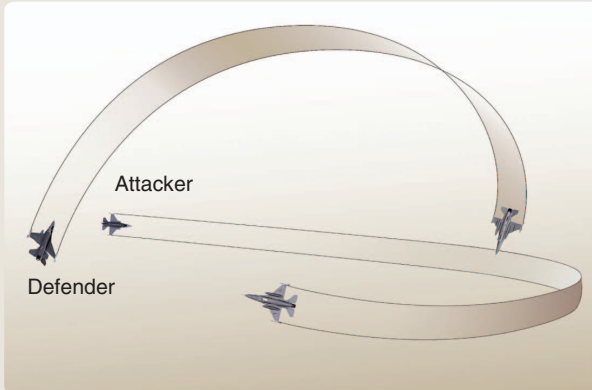


FIGURE S3 High yo-yo maneuver. The defender is vulnerable to the attacker at the initial position. The defender executes a sharp climbing-turning maneuver, rolls, and descends onto the trail of the attacker. At the final position, the defender has the advantage over the attacker.

cone of vulnerability; then the defender executes a high speed climbing turning maneuver to leave the critical area, while the attacker aircraft continues to turn in the defender's direction. At the final stage, the defender dives sharply to get in position behind the attacker, which results in interchange of their roles in combat. The split-S is a defensive maneuver, where the defender rolls the aircraft inverted and performs a half loop to leave the firing range of the fighter aircraft.

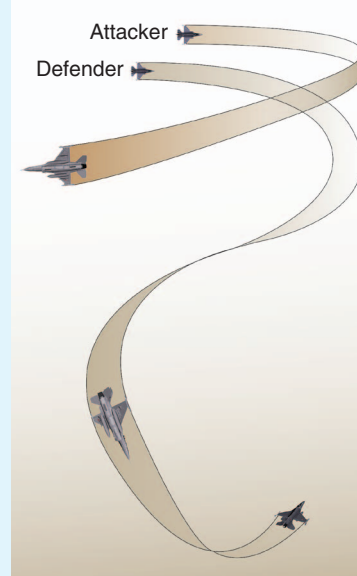


FIGURE S4 Split-S maneuver. The defender descends to exit the plane of the attacker and then rolls and draws a loop to reverse the aircraft's direction. At the end, the defender completely reverses its heading and avoids the threat.

as the primary choice in attitude parameterization and switch to quaternions only during numerical simulation to avoid these singularities. The angular velocity vector ω is consistently expressed in body axes as $[P, Q, R]^T$. The relationship between body-axes Euler angles, wind-axes Euler angles, and aerodynamic angles is displayed in Figure 3. More information on aircraft variables and sets of axes and transformations are available elsewhere [35].

The inputs of the aircraft, $\delta = [\delta_T, \delta_e, \delta_a, \delta_r]^T$, are the throttle setting and elevator, aileron, and rudder deflections. Additional actuators such as thrust vector devices and direct force control actuators can be considered to expand the set of feasible maneuvers for UCAVs; however, to preserve the applicability of the arguments within this article, we only consider conventional UAV control devices.

Rotations from one set of axes to another are expressed in terms of a direction cosine matrix. When three rotations

are performed in a yaw-pitch-roll sequence, the transformation matrix is

$$R(\alpha_1, \alpha_2, \alpha_3) = \begin{bmatrix} c\alpha_1 c\alpha_2 & c\alpha_1 s\alpha_2 s\alpha_3 - s\alpha_1 c\alpha_3 & c\alpha_1 s\alpha_2 c\alpha_3 + s\alpha_1 s\alpha_3 \\ s\alpha_1 c\alpha_2 & s\alpha_1 s\alpha_2 s\alpha_3 + c\alpha_1 c\alpha_3 & s\alpha_1 s\alpha_2 c\alpha_3 - c\alpha_1 s\alpha_3 \\ -s\alpha_2 & c\alpha_2 s\alpha_3 & c\alpha_2 c\alpha_3 \end{bmatrix} \quad (2)$$

where the letters s and c are abbreviations for the sine and cosine functions. Differential equations for the position variables in Cartesian coordinates are given by

$$\begin{bmatrix} \dot{n}_p \\ \dot{e}_p \\ \dot{h} \end{bmatrix} = R(\psi, \theta, \phi) \begin{bmatrix} U \\ V \\ -W \end{bmatrix}, \quad (3)$$

using body-axes velocity components. Using wind-axes Euler angles in both sequences results in

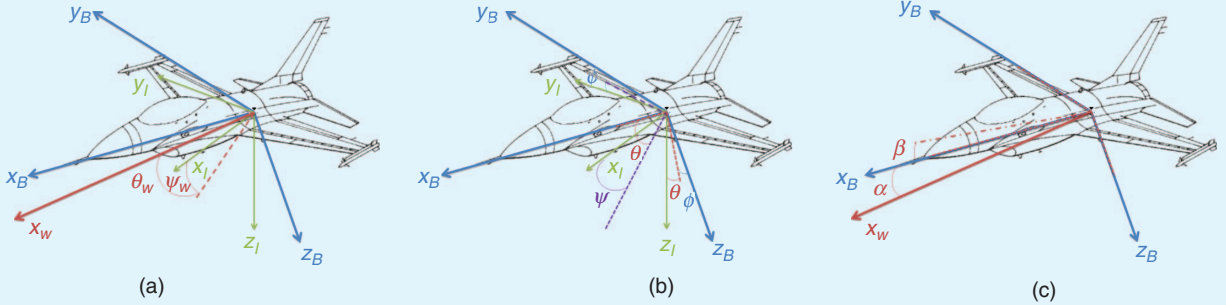


FIGURE 3 Relationship between different axes of the aircraft and Euler angles for transformation between them. The subscript I denotes the inertial axes, B denotes the body axes, and W denotes the wind axes. (a) Relationship between the inertial and wind axes. (b) Relationship between the body and inertial axes. (c) Relationship between the body and wind axes.

$$\begin{bmatrix} \dot{n}_p \\ \dot{\theta}_p \\ \dot{h} \end{bmatrix} = V_T \begin{bmatrix} c\theta_w c\psi_w \\ c\theta_w s\theta_w \\ s\theta_w \end{bmatrix} = V_T \begin{bmatrix} c\psi'_w c\theta'_w \\ s\psi'_w \\ c\psi'_w s\theta'_w \end{bmatrix}. \quad (4)$$

For lateral cylindrical coordinates, the differential equations are given by

$$\begin{bmatrix} \dot{r}_{lat} \\ r_{lat} \dot{\eta}_{lat} \\ \dot{h} \end{bmatrix} = V_T \begin{bmatrix} c\theta_w c(\eta_{lat} - \psi_w) \\ c\theta_w s(\eta_{lat} - \psi_w) \\ s\theta_w \end{bmatrix}, \quad (5)$$

again using standard wind-axes Euler angles. Reversed pitch-yaw sequence Euler angles are preferred in longitudinal cylindrical coordinates to express them in a simpler form

$$\begin{bmatrix} \dot{r}_{lon} \\ r_{lon} \dot{\eta}_{lon} \\ \dot{\theta}_p \end{bmatrix} = V_T \begin{bmatrix} c\psi'_w c(\eta_{lon} - \theta'_w) \\ c\psi'_w s(\eta_{lon} - \theta'_w) \\ s\psi'_w \end{bmatrix}. \quad (6)$$

Differential equations for the body-axis Euler angles and quaternions are

$$\begin{bmatrix} \dot{\psi} \\ \dot{\theta} \\ \dot{\phi} \end{bmatrix} = \begin{bmatrix} 0 & s\phi/c\theta & c\phi/c\theta \\ 0 & c\phi & -s\phi \\ 1 & s\phi t\theta & c\phi t\theta \end{bmatrix} \begin{bmatrix} P \\ Q \\ R \end{bmatrix}, \quad (7)$$

$$\begin{bmatrix} \dot{\beta}_0 \\ \dot{\beta}_1 \\ \dot{\beta}_2 \\ \dot{\beta}_3 \end{bmatrix} = \begin{bmatrix} 0 & -P & -Q & R \\ P & 0 & R & -Q \\ Q & -R & 0 & P \\ R & Q & -P & 0 \end{bmatrix} \begin{bmatrix} \beta_0 \\ \beta_1 \\ \beta_2 \\ \beta_3 \end{bmatrix}. \quad (8)$$

The relationship between the body-axes Euler angles, the wind-axes Euler angles, and the aerodynamic angles is

$$R(-\beta, \alpha, 0)R(\psi_w, \theta_w, \phi_w) = R(\psi, \theta, \phi), \quad (9)$$

where the explicit form of this relationship is in [36]. Finally, 6DOF nonlinear rigid body dynamics of the aircraft are represented by

$$m \begin{bmatrix} \dot{U} \\ \dot{V} \\ \dot{W} \end{bmatrix} = m \begin{bmatrix} 0 & -R & Q \\ R & 0 & -P \\ -Q & P & 0 \end{bmatrix} \begin{bmatrix} U \\ V \\ W \end{bmatrix} = mg \begin{bmatrix} -s\theta \\ c\theta s\phi \\ c\theta c\phi \end{bmatrix} + \begin{bmatrix} A_x \\ A_y \\ A_z \end{bmatrix}, \quad (10)$$

and

$$\begin{bmatrix} I_x & 0 & -I_{zx} \\ 0 & I_y & 0 \\ -I_{zx} & 0 & I_z \end{bmatrix} \begin{bmatrix} \dot{P} \\ \dot{Q} \\ \dot{R} \end{bmatrix} = \begin{bmatrix} 0 & -R & Q \\ R & 0 & -P \\ -Q & P & 0 \end{bmatrix} \begin{bmatrix} I_x & 0 & -I_{zx} \\ 0 & I_y & 0 \\ -I_{zx} & 0 & I_z \end{bmatrix} \begin{bmatrix} P \\ Q \\ R \end{bmatrix} + \begin{bmatrix} M_x \\ M_y \\ M_z \end{bmatrix}, \quad (11)$$

where m is the mass of the aircraft and g is the gravitational acceleration. A_x , A_y , and A_z correspond to the aerodynamic and thrust forces acting on each body axis. These forces are usually modeled as a function of velocity, altitude, angle of attack, sideslip angle, and control surface deflections. In many cases, an explicit form of these functions is not available, and they must be estimated from experimental data and stored in look-up table as given in [37]. In (11), I_x , I_y , I_z , and I_{zx} are the moment of inertias around the body axes and M_x , M_y , and M_z are the aerodynamic moments applied to the aircraft around each axis. Similar to the aerodynamic forces, the aerodynamic moments are also functions of velocity, altitude, angle of attack, sideslip angle, and control surface deflections.

Maneuver Modes and Modal Inputs

The state trajectory of a maneuvering aircraft can be described by forming a fixed state vector with variables chosen from the previous section. However, as noted previously, this approach may be redundant for most maneuvers of interest and introduces extra complexity to the controller design process. This section demonstrates how a library of maneuver modes and associated maneuver parameters can be built so that flight trajectories of interest can be represented as a sequence of maneuver modes instead of a time history of a single state vector.

To gain insight to the concept of parameterized maneuvers, consider a finite set of level-flight maneuvers, each with a different velocity. Compare this to a single mode labeled as level flight, parameterized continuously by the velocity. The later description has the advantage of creating a parameterized maneuver family spanning flight envelope

**This article treated the planning and control of agile maneuvers,
which is a key technology for UCAVs operating in
adversary environments.**

dynamics of the aircraft. Such parameters are referred to as *modal inputs* throughout the article. The extra challenge in this framework is identifying the necessary modes and modal input pairs required to cover a large class of aerobatics and combat maneuvers.

A natural question at this step is how to select the modal inputs for a specific maneuver mode. For this reason, note the following relations between the modal inputs, the initial conditions, and the DOF of the system. A maneuver mode is modeled as a nonlinear dynamical system with reduced order dynamics. The reduction comes from state constraints that arise due to the inherent dynamics of the maneuver mode. Consider the level-flight mode, which comes intuitively as the first primary maneuver mode of an aircraft. When the aircraft is flying in level-flight mode throughout a specific time interval, the aircraft is pictured as flying in a rectilinear path with a zero roll angle. However, this description is not sufficient because there are other state variables that need to be defined. For instance, the heading and altitude of the aircraft do not affect dynamics of the level flight as long as their rates are zero. Initially it is possible to accept altitude and yaw angle as a modal input to level-flight mode, but the fact that these variables are constrained to be constant during execution of the mode indicates that they add no insight to the evolution of the aircraft's states during the execution of this mode. These types of variables are modeled as initial conditions, and then their rate of change is constrained to be zero on the mode. Hence, altitude and heading are not a modal input to level-flight mode, and once they are given as initial conditions, they stay constant during the execution of the maneuver. Velocity is, however, a modal input to level flight since it can be adjusted freely during the execution of the mode. In addition to constrained variables, there are also driven states, which are effected directly by the modal inputs. For instance, in level-flight mode, the north and east positions evolve according to the velocity, which is the modal input for this mode.

An immediate advantage of working in a multimodal framework is the freedom to assign different state variables to each mode from the set of available state variable descriptions. The individual coordinate frame of each mode will be referred to as *modal coordinates*. The presentation of the evolution of states in a single coordinate frame is referred to as *global coordinates*. It is possible to develop forward and inverse transformations between modal and global

coordinates. These transformations can be used before and after the execution of each mode to obtain the evolution of states in global coordinates. For instance, it makes sense to assign cylindrical coordinates as modal coordinates to a turning flight mode, due to the fact that, for this mode, the position equations are described in a much simpler form in cylindrical coordinates. After the completion of a turning flight mode, the variables can be transformed back to global coordinates. For global coordinates, we use the state vector

$$X = [V_T \ \alpha \ \beta \ \varphi \ \theta \ \psi \ P \ Q \ R \ n_p \ e_p \ h]^T. \quad (12)$$

Based on the discussion on state constraints and coordinate transformations, a mathematically consistent formulation of maneuver modes and modal inputs may be given as follows. Given a nonlinear dynamical system in state-space form as in (1), a smooth and invertible coordinate transformation

$$\xi: \mathbb{R}^n \rightarrow \mathbb{R}^n, \quad (13)$$

maps the global coordinates X to local coordinates of the maneuver mode, Y . The states in the maneuver mode are decomposed into three subspaces, $Y: Z \times D \times M$, $Z \in \mathbb{R}^{n-l-k}$, $D \in \mathbb{R}^l$, and $M \in \mathbb{R}^k$. In this decomposition, Z represents the states that are constrained to be kept constant during the execution of the mode, D represents the states that are driven by modal inputs, and M is the set of modal inputs. In this context, a maneuver mode is a reduced order dynamical system given by

$$\dot{Z} = 0, \quad (14)$$

$$\dot{D} = h_1(D, M), \quad (15)$$

$$\dot{M} = h_2(D, M) + g_1(u). \quad (16)$$

The true inputs of the system are assumed to enter into the maneuver mode dynamics through the modal inputs space. As a result, the modal inputs can be controlled through a feedback control law of the form

$$u = k(D, M, Z). \quad (17)$$

Depending on the maneuver mode, a modal input can be time varying or constant. We show the time-varying modal inputs with (t) next to their symbols. Once the execution of the maneuver is completed, the trajectories of the system are obtained by performing the inverse coordinate

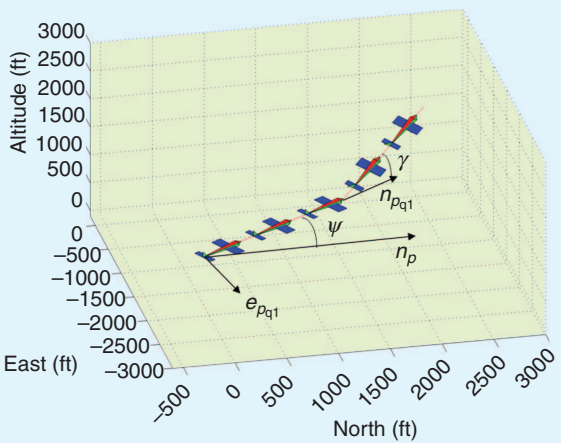


FIGURE 4 Level flight and climb/descent modes. In level-flight mode, the altitude is kept constant whereas the climb/descent is characterized by a constant altitude gain/loss rate. Both modes are characterized by a constrained attitude and driven position dynamics. These trajectories are parameterized by the velocity and climbing angle.

transformation ξ^{-1} . When multiple maneuver modes exist, we use subscript notation to distinguish between their coordinates, equations, and transformations.

Given a nonlinear system and a set of maneuver modes, the state-space trajectory of the system is replaced with the trio sequence given by

$$(q_i^j, m_i^j, \tau_i), \quad i = 1, 2, \dots, N, j \in \{1, \dots, N_m\}, \quad (18)$$

in which N is the number of modes in the mode sequence, N_m is the number of maneuver modes in the library, q_i^j is the j th maneuver mode of the system executed in i th order, m_i^j is the set of modal input values associated with the i th maneuver mode, and τ_i is the time duration of the i th maneuver mode. Equation (18) is referred to as a *modal sequence* throughout this article.

Although this framework does not necessarily limit the selection of the driven dynamics and the modal inputs, the most suitable choice for the nonlinear 6DOF aircraft dynamics consists of selecting position and attitude variables as driven and/or constrained dynamics, and translational and angular velocities as modal inputs. This situation is also the case for a wide class of mechanical systems, where the differential equations can be split into kinematic and dynamic equations.

Cruise Modes

Cruise modes consist of level flight and climb/descent modes that are characterized by a straight flight path with fixed heading and zero body angular rates. Although these kinds of trajectories are often referred to as *trimmed trajectories* in the context of aircraft stability and flight controls, the speed and pitch angle can be allowed to be varied during

the execution of these modes. This extra flexibility provides the capability to perform agile maneuvers such as accelerating level flight.

For cruise modes, the state vector of the original coordinates in (12) is used. A typical level-flight mode followed by a climb mode is shown in Figure 4 using local coordinates.

Level-flight mode is the most basic aircraft maneuver, where the aircraft flies at a fixed heading and altitude while keeping wings level with zero roll angle. A commercial aircraft spends most of its route in this mode since it is the most convenient way to fly from one point to another while keeping altitude constant. The symbol q_1 represents the level-flight mode.

Using (14)–(16), the variables and the constraints of this mode are

$$Z_{q_1} = \{e_p, h, \phi, \psi, \beta, P, Q, R\}, \quad (19)$$

$$D_{q_1} = \{n_p, \theta = \alpha\}, \quad (20)$$

$$M_{q_1} = \{V_T(t)\}. \quad (21)$$

To simplify the notation, the subscript q_1 is dropped from the states, and the subscript is only included on the notation of the sets. Velocity selection is the only degree of freedom for the level-flight mode and hence the only modal input. The velocity is allowed to be time varying in this case except the altitude rate, which is constrained to be zero. As a result, this mode contains not only trimmed level flight but also the acceleration and deceleration maneuvers. These two maneuvers are critical for the aircraft to gain or to lose kinetic energy during agile maneuvering.

The climb/descent mode is also one of the most commonly encountered maneuvers used for gaining or losing altitude. In commercial flight, this maneuver is performed during take-off and landings. In aerobatics and air combat, sharp climbs and descents are commonly performed to trade airspeed with altitude. A typical descent and coordinate transformation is displayed in Figure 4. The symbol q_2 is used to represent the climb/descent mode.

Using the context of (14)–(16), the variables and the constraints of this mode are

$$Z_{q_2} = \{e_p, \phi, \psi, \beta, P, Q, R\}, \quad (22)$$

$$D_{q_2} = \{n_p, h, \theta\}, \quad (23)$$

$$M_{q_2} = \{V_T(t), \gamma = \theta - \alpha\}. \quad (24)$$

Three-Dimensional Modes

Out-of-plane maneuvers are essential to agile flight, as they not only provide extensive usage of the lateral plane but also provide an unexpected tactical advantage in air combat. Three-dimensional (3D) maneuvers involve angular motion around all axes, and they are performed under high g forces. At first glance, it may seem like there are no

constrained states for these modes; however, it is possible to identify the constrained states by using cylindrical coordinates and wind-axes Euler angles. In addition, this specific coordinate and angle representation set gives a simpler and more elegant description of the associated states and modal inputs for the out-of-plane maneuvers. Three-dimensional maneuvers are categorized into two classes: lateral loops and longitudinal loops. In both modes, local coordinates use the cylindrical coordinates for position representation and velocity-related variables are converted to wind-axes Euler angles by using (9).

Reviewing each of the possible modes one by one, the lateral-loop mode corresponds to drawing a loop on the lateral plane of the aircraft. This maneuver becomes an out-of-plane maneuver when combined with altitude loss or gain. Such loops are commonly executed to change the heading of the aircraft. A special case of a lateral loop is known as a *coordinated turn*, which is a constant-altitude constant-velocity lateral plane turn. It is a regular maneuver performed by commercial aircraft to change the heading during cruise. Three-dimensional lateral loops such as turning climbs are performed by fighter aircraft to leave the plane of combat or trade speed for altitude. The lateral-loop mode is referred to as q_3 , with dynamics given by

$$Z_{q_3} = \{r_{\text{lat}}, \beta\}, \quad (25)$$

$$D_{q_3} = \{\eta_{\text{lat}}, h, \alpha, \phi_w, P, Q, R\}, \quad (26)$$

$$M_{q_3} = \{V_T(t), \theta_w, \dot{\psi}_w\}. \quad (27)$$

To see how wind-axes Euler angles influence geometry of the mode, see Figure 5. While V_T and constant rate $\dot{\psi}_w$ shape the radius of the loop and position of the aircraft on the loop, the constant pitch angle θ_w determines how the velocity vector bends the flight path during the maneuver. For example, zero pitch angle corresponds to a coordinated turn and positive pitch angle results in a turning climb.

Drawing loops in the longitudinal plane is encountered frequently in aerobatics. These two-dimensional maneuvers can be expanded by adding Euler yaw angle in wind axes as a modal input. With this modal input, maneuvers like a barrel roll, which can be defined as a loop around an imaginary cylinder with a base in the longitudinal plane and extends into the lateral axis of the aircraft, can be defined. The longitudinal loop mode is denoted as q_4 , with dynamics given by

$$Z_{q_4} = \{r_{\text{lon}}, \beta\}, \quad (28)$$

$$D_{q_4} = \{\eta_{\text{lon}}, e_p, \alpha, \phi'_w, P, Q, R\}, \quad (29)$$

$$M_{q_4} = \{V_T(t), \dot{\theta}_w, \psi'_w\}. \quad (30)$$

Similar to the lateral loop mode, the longitudinal loop mode makes use of cylindrical coordinates, but in reverse sequence wind-axes Euler angles. In Figure 6, it is seen that zero yaw angle corresponds to the vertical loop, while

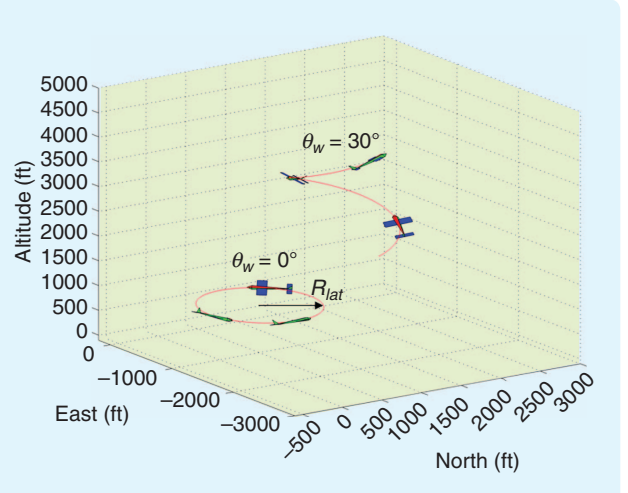


FIGURE 5 Lateral loops with zero and nonzero wind axes pitch angles. Zero pitch angle refers to a coordinated turn, with zero altitude change. Nonzero pitch angles result in coordinated climbing-turning maneuvers, which are commonly encountered in air combat.

barrel roll-like maneuvers can be described with nonzero yaw angles.

Attitude Transition Modes

Cruise modes, along with loop modes, serve as a modular library to navigate in a three-dimensional environment. Since the path of a UCAV is not a modal input to any of the modes, path continuity in a modal sequence is always satisfied. However, the attitude of the aircraft is not necessarily continuous between mode transitions. To resolve this issue, two controlled attitude transition modes are presented that are inspired from the literature on aerobatics [31] and literature on attitude parameterization for large attitude aerobatic maneuvers [38]. The main use of these

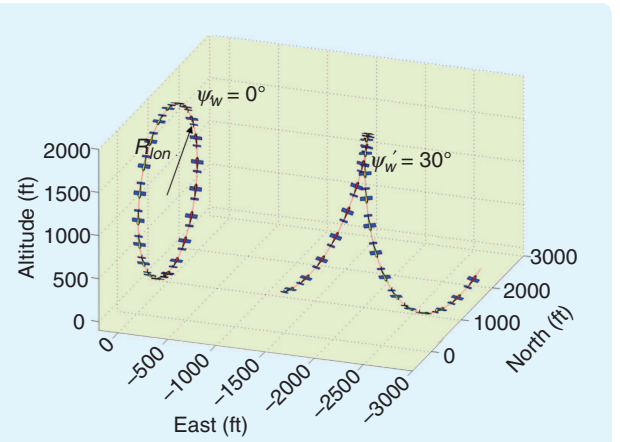


FIGURE 6 Longitudinal loop modes with zero and nonzero wind axes yaw angles. Zero yaw angle refers to vertical loops in longitudinal plane. Such loops are an integral part of aerobatics. Nonzero yaw angles result in cylindrical trajectories, which are also known as barrel rolls in aerobatics and air combat.

modes is to create a smooth attitude transition during maneuver mode switches.

The standard description of attitude dynamics defined relative to a fixed global frame is not useful to handle mode transitions, which instead are handled using a relative attitude transformation between maneuver modes. For this purpose, roll, pitch, and yaw angles $\{\phi_r, \theta_r, \psi_r\}$ are used [38]. The time derivative of these variables serve as a set of modal inputs for attitude transition modes. These angles can be interpreted as being the required angular displacements to make a smooth attitude transition. More information on the dynamics of these variables are described elsewhere [38].

The simultaneous control of all three attitude angles is possible through coordinated control of the aileron, rudder, and the elevator deflections. However, this approach is rarely utilized in practice, and the fighter pilots adjust their nose pointing angle and roll angle separately [31]. Two modes are presented here that can be executed sequentially to point the aircraft and its velocity vector at the right direction while switching between maneuver modes.

As described above, the main aim of the pitch/yaw transition mode is to point the UCAV in the right direction in terms of body-axes Euler pitch and yaw angles. For example, these kind of transitions are required when switching from level flight to steep climbs. This mode is referred to as q_5 , with dynamics given by

$$Z_{q_5} = \{n_p, e_p, h, V_T, \phi\}, \quad (31)$$

$$D_{q_5} = \{\theta, \theta_w, \psi, \psi_w\}, \quad (32)$$

$$M_{q_5} = \{\dot{\theta}_r(t), \dot{\psi}_r(t)\}. \quad (33)$$

As seen in (31), attitude transitions are assumed to be executed fast enough to be able to neglect the change in the position of the aircraft during the execution of this mode. Driven dynamics are selected as the pitch and the yaw angles in body and wind axes. These two variables are adjusted to desired values by driving them with modal inputs, namely, the pitch rate and yaw rate. This particular selection of modal inputs is analogous to the selection of

translational velocity components as modal inputs on cruise and looping modes.

As most of the loops result in either inverted or unusual roll attitude, roll transitions of the aircraft in between maneuvers is a common practice in aerobatics [32]. Roll maneuvers also have applications in air combat. For example, in the Immellman turn, the aircraft becomes inverted at the end of the loop and has to roll 180° to regulate back into the level-flight mode. The last mode corresponds to the roll motion and is referred to as q_6 . The dynamics of the roll mode are

$$Z_{q_6} = \{n_p, e_p, h, \theta, \psi, V_T, \beta\}, \quad (34)$$

$$D_{q_6} = \{\alpha, \phi\}, \quad (35)$$

$$M_{q_6} = \{\dot{\phi}_r(t)\}. \quad (36)$$

Similar to the other transition modes, the position of the UCAV is not subject to the particular path control during roll mode. This time, the pitch and the yaw angles are kept constant, and the roll angle is regulated to a desired value through angular velocities.

Complete Maneuver Library

The maneuver modes and modal inputs are summarized in Table 1. This table does not capture the full lateral characteristics of the aircraft because the sideslip angle is constrained to be zero on every mode and potential modes like sideslip flight are discarded for brevity. Another design choice is the exclusion of rolling maneuvers such as aileron rolls and rolling circles, as the roll mode in Table 1 only acts as a transition mode. However, these specific maneuvers are not critical exclusions since most of the maneuvers described in [31] and [34] can be covered by a sequence of modes listed in Table 1.

As discussed during the development of the maneuver library, most aerobatic and combat maneuver sequences consist of concatenation of cruise and 3D modes, while the attitude modes are inserted in between mode switches for smooth attitude transitions. This argument leads to categorization of the cruise and 3D modes as primary modes

TABLE 1 Complete list of maneuver modes and modal inputs. The table summarizes constrained and driven states decomposition for each mode and modal inputs associated for each mode.

ID	Mode	Constrained States Z	Driven Dynamics D	Modal Inputs M
q_1	Level flight	$e_p, h, \phi, \psi, \beta, P, Q, R$	$n_p, \theta = \alpha$	$V_T(t)$
q_2	Climb/descent	$e_p, \phi, \psi, \beta, P, Q, R$	n_p, h, θ	$V_T(t), \gamma = \theta - \alpha$
q_3	Lateral loop	r_{lat}, β	$\eta_{lat}, h, \alpha, \phi_w, P, Q, R$	$V_T(t), \theta_w, \psi_w$
q_4	Longitudinal loop	r_{lon}, β	$\eta_{lon}, e_p, \alpha, \phi'_w, P, Q, R$	$V_T(t), \dot{\theta}'_w, \psi'_w$
q_5	Pitch-yaw transition	n_p, e_p, h, V_T, ϕ	$\theta, \theta_w, \psi, \psi_n$	$\dot{\theta}_r(t), \dot{\psi}_r(t)$
q_6	Roll	$n_p, e_p, h, \theta, \psi, V_T, \beta$	θ, ϕ	$\dot{\phi}_r(t)$

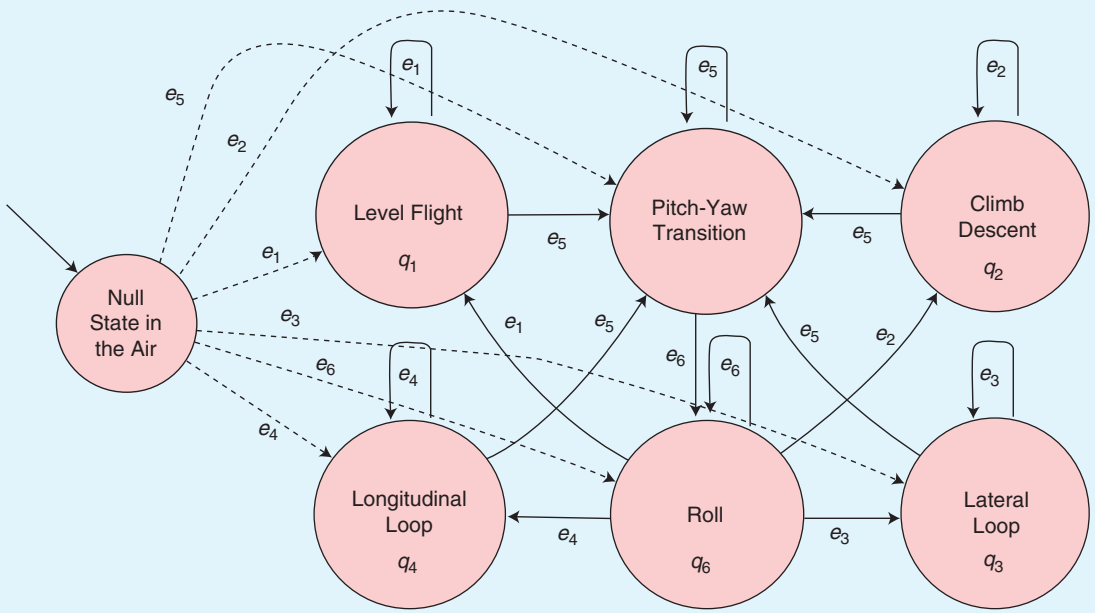


FIGURE 7 The complete maneuver library with transition diagrams between the modes. Maneuver sequences usually consist of a concatenation of four primary modes q_1, q_2, q_3, q_4 with attitude transition modes q_5, q_6 inserted in between.

$q_1 - q_4$ and the categorization of the attitude modes as transition modes q_5, q_6 . Figure 7 displays the maneuver modes and the associated transitions across these modes.

MULTIMODAL FLIGHT CONTROL ON SLIDING MODES

The maneuver decomposition methodology as explained in the associated section showed that it is possible to break up arbitrary maneuvers into a sequence of maneuver modes. Since the dynamics of each mode may have different constraints and different tracked variables, this natural decomposition allows the consideration of the UCAV agile maneuvering controller design problem as a) designing a specific controller to each mode and b) switching between the specific controls in synchronization with the modes of the maneuver sequence.

The modal dynamics in Table 1 provide an intuitive insight to the controller design process. Since modal inputs shape the trajectory of each maneuver mode, then these modes could indeed be regulated with a local controller specific to each maneuver mode/modal input pair. Thus, the first objective of each local controller is to keep the modal error tracking error

$$e_m(t) = \hat{m}_j(t) - m_j(t), \quad t \in \tau_j \quad (37)$$

as close to zero as possible, where $m_j(t)$ refers to the modal input of the j th mode of the sequence and $\hat{m}_j(t)$ refers to the dynamics variable of the actual system corresponding to the modal input. Equation (37) states that the modal inputs corresponding to that mode must be tracked within the time interval of that specific mode. For example, if the

corresponding mode is the level-flight mode, then the total velocity, which is entered as a modal input to the mode, must act as a reference desired value for the velocity controller system and the controller must regulate the total velocity to the value of the modal input during execution of the mode.

The second objective of the controller is to satisfy constraints in (14). These constraints arise from the state constraints that determine the path and the attitude of the aircraft during execution of the maneuver. This control objective is defined by

$$\dot{\tilde{Z}}_j = 0, \quad t \in \tau_j. \quad (38)$$

If the controller satisfies (37) and (38), the driven dynamics in (15) coincide with the actual dynamics of the system, and then the aircraft exhibits the desired behavior. The overall diagram of the UCAV control system is in Figure 8.

Overall, the problem as presented is an underactuated nonlinear control problem in which there exists a subset of variables that must be regulated to reference values and the remaining subset of variables must be kept bounded. This problem can be addressed using tools from variable structure control theory [19]. The basic idea of SMC is to design a sliding surface $\sigma(x)$ such that, once the system is on the sliding surface, the dynamics exhibit the desired behavior. Later, this surface is rendered as invariant by choosing an appropriate control law. This design philosophy fits to multimodal maneuvering framework nicely since the driven and the constrained states of each maneuver mode can be cast as a lower dimensional hypersurface in the state space.

There are two main limitations of the classical SMC that prevents its direct application to the maneuver control problem. The first limitation results from the NMP outputs that appear during the controller design of the cruise and the 3D maneuvering modes. Direct SMC design to control the translation-related variables (such as velocity and loop radius) results in unstable attitude dynamics, so SMC design is not feasible for the cruise and the 3D maneuvering modes. A second limitation is the resultant chattering from the SMC as it generates high frequency input signals that cannot be tracked by actuators. Both of these issues are handled by exploiting two modern SMC techniques. The NMP output problem is handled by breaking down the whole control scheme to an inner-outer loop architecture and handling the effect of NMP outputs by a variant of SMC known as *dynamic sliding mode control* (DSMC). The chattering problem, which is now moved to the inner loop, is handled by using higher order sliding mode (HOSM) control. For more information on HOSM, see "Higher Order Sliding Mode Control."

Design for Cruise and Looping Modes via Dynamic Sliding Mode Control

The common design property of these modes is the need for precise control of the aircraft path during maneuvers. In cruise modes, no lateral movement is allowed, and the rate change of altitude and attitude must be kept constant in

order to satisfy state constraints. For looping modes, both the path and the attitude of the aircraft must be controlled precisely for efficient tracking of the modal inputs.

For cruise modes, the controlled outputs are set as

$$C_{q1} = C_{q2} = \{V_T, \gamma, \phi, \beta\}. \quad (39)$$

Examining (39), note that the modal inputs of level and climb/descent modes (V_T and γ) enter into the controlled output sets directly, while the rest of the outputs are selected as lateral variables to satisfy the state constraints of $\beta = 0$ and $\phi = 0$. These state constraints correspond to no sideslip and wings level condition.

For lateral and longitudinal loop modes, the controlled output set is

$$C_{q3} = \{V_T, \theta_w, \dot{\psi}_w, \beta\}, \quad (40)$$

$$C_{q4} = \{V_T, \dot{\theta}_w, \dot{\phi}_w, \beta\}. \quad (41)$$

The modal inputs in (25)–(27) and (28)–(30) enter directly into the controlled output set and the variable β is controlled to achieve coordinated flight. For the analysis, the dynamic equations of the aircraft can be put into a compact form such as

$$\dot{V} = f_1(V)\omega + f_2(\theta) + g_1(V)\delta_T + g_2(V)[\delta_e, \delta_a, \delta_r]^T, \quad (42)$$

$$\dot{\omega} = f_3(V) + f_4(\omega) + g_3(V)[\delta_e, \delta_a, \delta_r]. \quad (43)$$

The explicit form of these equations can be recovered from the section "Maneuver Decomposition Methodology." Unfortunately, as noted in the introduction of this section, direct SMC design is not possible for the system in (42) because of the NMP properties of outputs in (39)–(40). This phenomenon, as previously noted by researchers in [39] and [40], arises due to the fact that the control surfaces $[\delta_e, \delta_a, \delta_r]$ creates moments while regulating velocity variables in (42). Basically, direct SMC design tries to track velocity variables through these control surfaces, which in turn renders the attitude dynamics unstable through the moments created by the control surfaces.

To overcome this problem, the vector $[\delta_T, P, Q, R]$ is modeled as a virtual input signal to (42), while accepting the effect of control surfaces, $g_2(V)$, as an external disturbance to the system. Then this disturbance is rejected through utilization of DSMC design. Once the required angular velocities are calculated through this loop, they can be fed as a reference to a separate loop. This inner loop is based on the angular dynamics of (43), in which $[\delta_e, \delta_a, \delta_r]$ is computed to track the reference angular velocities provided by the outer loop. The overall diagram for this inner-outer loop approach can be seen in Figure 9.

To illustrate the design process, the DSMC design is presented here for the longitudinal loop mode (the design for the other modes is analogous). Let $V = [V_T, \theta_w, \dot{\psi}_w, \beta]$ represent the controlled variables, and let $u_o = [\delta_T, P, Q, R]$

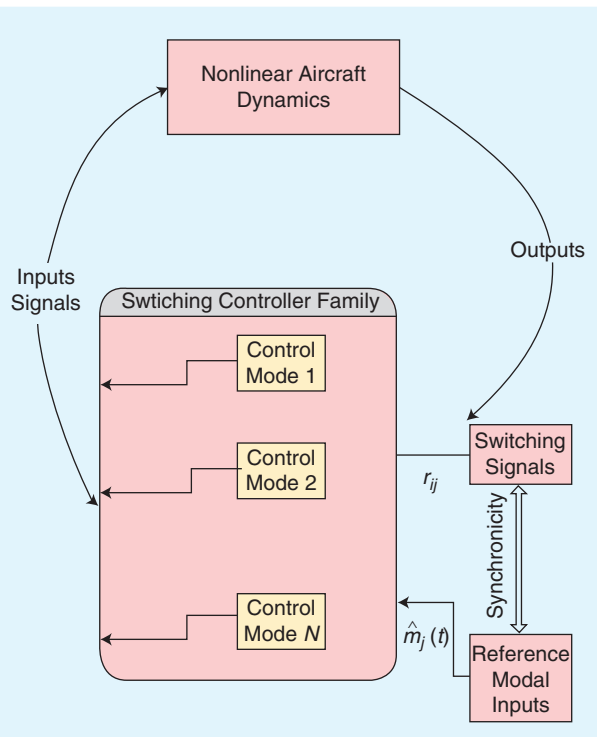


FIGURE 8 Switched control system diagram. The switching sequence given by the flight planner is synchronized to the switching sequence and to the controllers. Each controller is designed for local control of a specific maneuver mode.

Higher Order Sliding Mode Control

The basic idea of sliding mode control (SMC) defines a sliding surface $\sigma(x) = 0$ for the controlled system, where the system evolves according to a desired behavior on the surface. After selecting the sliding surface, the control law is designed such that sliding surface becomes attractive surface. This is achieved by enforcing the sliding condition $\sigma\dot{\sigma} < 0$, and thus turning the sliding surface to invariant as seen in Figure S5. Classical sliding mode control is known to generate high-frequency control signals to enforce the sliding condition while under disturbances. This phenomenon is usually called *chattering*, which is briefly illustrated in Figure S6.

Higher order sliding modes (HOSM) enforce higher order derivative constraints on the sliding surface, while keeping the advantages of the classical SMC. HOSM control removes chattering completely and provides better control accuracy and robustness [48], [49]. The r th order sliding mode can be defined by

$$\sigma = \dot{\sigma} = \ddot{\sigma} = \dots = \sigma^{(r-1)} = 0, \quad (\text{S1})$$

which forms an r -dimensional constraint set on the dynamics of the system.

Two of the most common HOSM design approaches are twisting and supertwisting algorithms [49]. Here we describe how twisting algorithm can be applied to a single-input single-output nonlinear system. For the state vector x and input signal u , the dynamics of the system are given as

$$\dot{x} = f(x) + g(x)u, \quad (\text{S2})$$

where f and g are sufficiently smooth functions. The designer selects an appropriate sliding surface $\sigma(x)$ such that, whenever $\sigma(x(t)) = 0, t \geq t_0$ for some time t_0 , the system exhibits the desired behavior. The next step is to find the equivalent control u_{eq} such that $\dot{\sigma}(x, u_{\text{eq}}) = 0$. Such a control law is usually computed by first calculating the derivative of the sliding surface $\dot{\sigma}(x) = (\partial\sigma/\partial x)(f(x) + g(x)u_{\text{eq}}) = 0$, and then extracting u_{eq} by inverting the system dynamics, $u_{\text{eq}} = g^{-1}(x) - f(x)$. Assume that u_{eq} is bounded above uniformly by U_M , which is usually estimated from simulations. The following control law [49], which is usually referred to as the *twisting algorithm*, ensures the realization of second-order sliding mode,

$$\dot{u} = \begin{cases} -u, & \text{if } |u| > U_M \\ \alpha_m \text{sgn}(\sigma), & \text{if } \sigma\dot{\sigma} \leq 0, |u| \leq U_M \\ \alpha_M \text{sgn}(\sigma), & \text{if } \sigma\dot{\sigma} > 0, |u| \leq U_M \end{cases} \quad (\text{S3})$$

in which $\alpha_M > \alpha_m > U_M$. More on the analysis of these types of control laws and their variants can be found in [49].

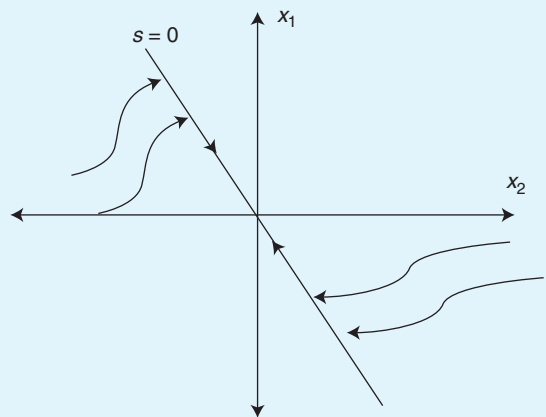


FIGURE S5 A sliding surface in the phase plane. The design objective is to make the sliding surface attractive so that the trajectories converge to the sliding surface asymptotically. The surface is selected such that, when the dynamics of the system are enforced to stay on the sliding surface, the system exhibits the desired behavior.

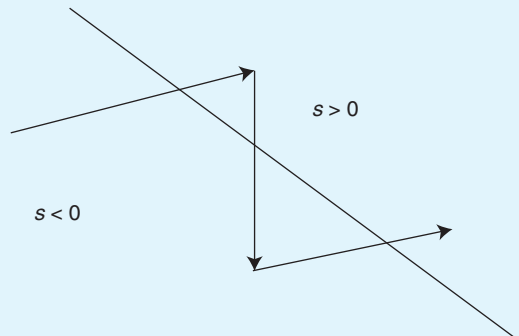


FIGURE S6 Chattering effect. Uncertainty and disturbances in the plant dynamics may perturb the sliding motion, thus the control signal must alter its sign based on the location of the current state with respect to the sliding surface. In the vicinity of the sliding surface, such perturbations may lead to high frequency oscillations with periodic changes on the sign of the input signal.

Two striking properties of HOSM control are to be noted. First, since the sign function is moved into the derivative of the control input, the chattering effect on the actual input signal is considerably weakened, without sacrificing any robustness or accuracy. Second, due to additional constraints in the sliding mode equations, disturbance rejection on the sliding surface is strengthened substantially.

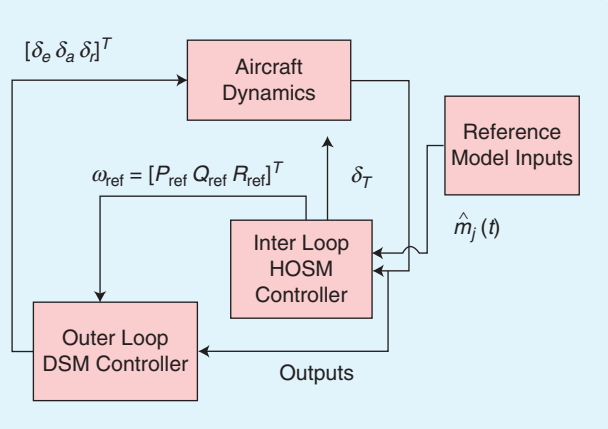


FIGURE 9 The control diagram for cruise and 3D modes. The outer loop generates the required angular velocities from modal inputs using dynamic sliding mode design, while the inner loop tracks these velocities to regulate the aircraft to stay within the commanded maneuver mode with the higher order sliding modes controller.

denote the virtual input signal. Equation (42) can be re-written as

$$\dot{V} = \hat{f} + (g + \Delta g) u_o + \hat{w}, \quad (44)$$

where $\hat{f} = f_2(\theta)$, $g = [f_1, g_1]$, $\hat{w} = g_2(V)[\delta_e, \delta_a, \delta_r]^T$, Δg represents the unknown dynamics/disturbances in the thrust input channel, and \hat{w} is the external disturbance to the system. Next, the sliding surfaces are defined for each output separately

$$\sigma_i = (V_i^d - V_i) + c_i \int (V_i^d - V_i) dt, \quad i = 1, \dots, 4, \quad (45)$$

in which V^d is the desired modal inputs, and scalar constants c_i are selected such that the characteristic polynomial for the differential equation $(\dot{V}_i^d - \dot{V}_i) + c_i(V_i^d - V_i) = 0$ is Hurwitz. Finally, assuming that g_1 is invertible in the domain of interest, by using multi-input, multi-output (MIMO) SMC theory [19], the control law can be calculated as

$$u_o = u_{eq} + K g^{-1} \text{sgn}(\sigma), \quad \sigma = \text{diag}(\sigma_i), \\ K = \text{diag}(k_i), \quad i = 1, \dots, 4, \quad (46)$$

where $u_{eq} = g^{-1} \hat{f}$, $\text{sgn}(\cdot)$ is the sign function, and the k_i are the appropriate control gains. The gains are selected by examining the Lyapunov function of the sliding surface. Let the positive-definite Lyapunov candidate be given as $U = 1/2 \sigma^T \sigma$. The time derivative of this Lyapunov function is

$$\begin{aligned} \dot{U} &= \sigma^T (\dot{V}^d - \hat{f} + (g + \Delta g) u_o + \hat{w} + C(V^d - V)) \\ &= \sigma^T (\dot{V}^d - (\hat{f} + \hat{w} + (g + \Delta g)(u_{eq} + K g^{-1} \text{sgn}(\sigma))) + C(V^d - V)) \\ &= \sigma^T (\mu - K(I + \Delta g g^{-1}) \text{sgn}(\sigma)), \end{aligned} \quad (47)$$

where $\mu = \dot{V}^d - \hat{f} - \hat{w} + C(V^d - V) - (I + \Delta g g^{-1})(\dot{V}^d - \hat{f} + C(V^d - V))$. It is assumed that μ and $\Delta g g^{-1}$ are bounded, so there exists a finite matrix \bar{g} and vector $\bar{\mu}$ such that $|\mu_i| < \bar{\mu}_i$, $|\Delta g g^{-1}| < \bar{g}_{ij}$, $i, j = 1, 2, 3, 4$. These bounds are usually estimated by using numerical simulations. Furthermore, the following choice of k_i ensures that the time derivative of the Lyapunov function candidate is negative definite:

$$k_i > \max_i \frac{\bar{\mu}_i + \eta_i}{1 - \sum_{j=1}^4 \bar{g}_{ij}}, \quad (48)$$

where $\eta_i > 0$ such that $\dot{U} \leq - \sum_{i=1}^4 \eta_i |\sigma_i|$.

Design for Attitude Transition Modes via Higher Order Sliding Modes

For attitude transition controllers, the required modal inputs can be found by transforming the roll, pitch, and yaw rates and relative Euler angles to body angular velocities. The selected controlled outputs are the same for both modes, as

$$C_{q5} = C_{q6} = \{P, Q, R\}. \quad (49)$$

The attitude transition controller is illustrated in Figure 9 as the inner-loop control system. This inner loop is integrated with the outer loop for controlling cruise and 3D maneuver modes, whereas the inner loop serves as a stand-alone control system for attitude transition maneuvers.

As noted previously, the main design issue for this loop is to avoid chattering in the control surfaces. For this purpose, an HOSM controller is utilized using a MIMO variant of the twisting algorithm described in “Higher Order Sliding Mode Control.” Similar to the outer-loop design, define the sliding surfaces λ as

$$\lambda_i = (\omega_i^d - \omega_i), \quad i = 1, 2, 3, \quad (50)$$

in which ω^d is the reference angular velocities generated by the outer loop. By inverting $g_3(V)$ in (43), the input channels can be decoupled from each other. Let $v = g_3^{-1} [\delta_e, \delta_a, \delta_r]$, then HOSM condition can be satisfied using the twisting algorithm:

$$\dot{v}_i = \begin{cases} -v_i, & \text{if } |v_i| > V_M \\ \alpha_m \text{sgn}(\lambda_i), & \text{if } \lambda_i \dot{\lambda}_i \leq 0, |v_i| \leq V_M \\ \alpha_M \text{sgn}(\lambda_i), & \text{if } \lambda_i \dot{\lambda}_i > 0, |v_i| \leq V_M \end{cases} \quad (51)$$

for $i = 1, 2, 3$. The values of the constants V_m, α_m, α_M should be tuned according to bounds on the functions f_3, f_4, g_3 ; however, in practice these values are tuned from simulation results based on the efficiency of the tracking performance. Once the pseudoinputs v_i are computed, they can be transformed back to the actual input signals $[\delta_e, \delta_a, \delta_r]$ through multiplication by $g_3(V)$. The HOSM design removes the chattering from input signals while increasing

One of the most critical planning problems for UAVs involve generating dynamically feasible obstacle-free paths in a cluttered environment.

robustness to unmodeled dynamics by enforcing the second-order HOSM condition $\lambda_i = \dot{\lambda}_i = 0$.

APPLICATIONS

Until now, we have shown how a specific library of maneuver modes and associated parameters can be developed to generate maneuver sequences based on aerobatics and air combat and how a family of switching nonlinear controllers can be designed to control each mode. This section presents two applications where the developed framework can be used to solve challenging planning and control problems for agile aircraft.

The first application, taken from [41], examines the problem of navigating in a dense environment and investigates how the developed framework can be integrated with a flight path planner to generate a feasible path in an heavily cluttered environment. The focus on this application is on the planning facet of the problem.

The second application focuses on the control facet by executing a sequence of challenging predefined aerobatic maneuvers. This application aims to demonstrate the tracking capability of the developed switching control system.

Both applications use a high-fidelity nonlinear 6DOF F-16 aircraft model provided in [37]. This model provides an extensive database of the aerodynamic forces/moments on the aircraft including high angle of attack regimes, which is of particular interest to agile maneuvering. The database also comes with a turbofan engine model that captures the effects of altitude and Mach number on the engine dynamics. It is important to verify aircraft control and planning algorithms on such a high-fidelity model since such a model allows us to see the limitations of the developed approaches on realistic agile flight situations, such as stall and control surface/engine saturation.

Integration with a Flight Path Planner: Navigation in Dense Environments

One of the most critical planning problems for UAVs involve generating dynamically feasible obstacle-free paths in a cluttered environment. Such problems are usually tackled by generating an obstacle-free path by using a kinodynamic path planner that utilizes a simplified version of vehicle dynamics [42], [43]. Later, the generated path is fed as a reference to a feedback control layer. However, such an approach can result in improper/infeasible maneuvers, especially if the obstacle density of the environment forces the aircraft to perform agile maneuvers such as tight turns or sudden altitude changes.

With this motivation in mind, a hierarchical control scheme is examined where an extra layer is inserted between the path planner and feedback control layers. This extra layer is called the *maneuver planner*, and its objective is to convert the time-parameterized flight path provided by the path planner to a modal sequence as in (18). An evident advantage of this approach is its ability to treat the feasibility of each maneuver mode separately rather than treating the feasibility of the overall maneuver. In addition, once a feasible modal sequence is found, it can be executed by switching between the control laws described in the previous section. Overall, this extra planning layer redefines the planned trajectory in terms of an agile aircraft motion instead of directly forcing UCAV to track a predesigned trajectory. This hierarchical control scheme is illustrated in Figure 10.

The pseudocode for the maneuver planning layer is provided in Algorithm 1. In summary, the main principle of the algorithm is first to extract primary modes identifying wind-axes Euler angles and then to insert attitude transition modes in between the identified modes to make the overall maneuver sequence feasible. For brevity, a basic description is presented here. A detailed treatment of maneuver sequence construction and feasible modal input selection problem is available elsewhere [41], [44].

The first two steps in Algorithm 1 describe the input and the output of the maneuver planner. In Step 3 of Algorithm 1, first the obstacle-free flight path is discretized into intervals with uniform time length, and then wind-axis Euler angles are computed by approximating the derivatives of the flight path with finite time differences using (4).

In the next step, the trajectory of wind-axis Euler angles is used to label the segments (i.e., modes) of the flight path, according to the constrained and driven variables of each mode as described in Table 1. For instance, if ψ_w and θ_w are fixed across a time interval, the algorithm identifies this segment as a cruise mode and, if $\theta_w = 0$ exactly, then the mode is identified as the level-flight mode.

The next step is to determine the feasible modal input for each of the labeled modes. For this purpose, we use a database of feasible modal input/angle of attack pairs specific to each mode, obtained by either simulation or through flight tests of the operating aircraft. Since collecting all the feasible modal input and angle of attack values over the full flight envelope of the aircraft can be intractable, the database is restricted as to the selection of the modal input/angle of attack pairs that output more aggressive maneuver profiles. Here, aggressiveness of each maneuver mode is measured using an agility metric. This metric is defined exclusively

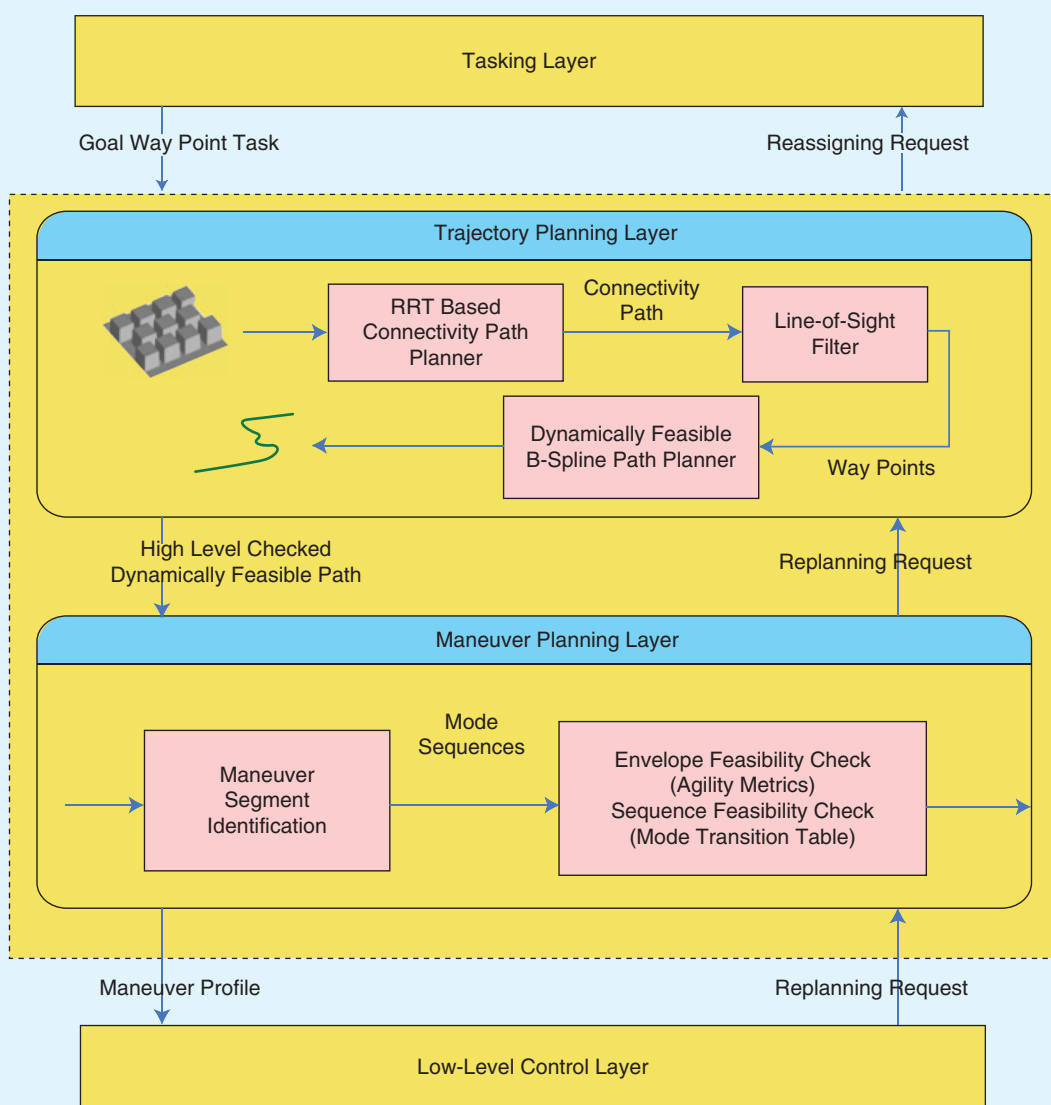


FIGURE 10 Integrated planning architecture for an unmanned combat air vehicle mission. The path-planning layer feeds the maneuver-planning layer that creates a feasible modal sequence based on the multimodal maneuvering framework defined in the article. This sequence is sent to the low-level control layer, in which the trajectory is tracked through a nonlinear switching controller structure.

for each mode, taking into account the individual dynamics and the associated aerobatics/air combat value. More information on agility metrics and how they are used in this framework can be found in “Agility Metrics.”

In the final step of the algorithm, the relative attitude jumps between a mode transition is determined using angle of attack and wind-axis Euler angle trajectories from (9). These attitude jumps are smoothed by inserting attitude transition modes in between the switching modes. The modal inputs of these modes are also selected from agility metric tables. The execution time interval of these transition modes are prespecified to the algorithm, and the execution time is based on the actuator saturation limits of the aircraft model. Since the attitude dynamics of aircraft

usually evolve on a relatively faster time scale, the effect of transition time intervals on the overall maneuvering time usually can be ignored.

The simulations consider a $200 \times 200 \times 200$ unit cube complex urban environment. In the first part, the path planning layer constructs a 3D time-parameterized flight path that avoids the obstacles while satisfying the velocity and acceleration constraints, by checking the flight envelope constraints. This time-parameterized flight path is then passed to the maneuver planning layer. An example solution of the path planner in the 3D urban environment is shown in Figure 11.

The maneuver planning algorithm decomposes the path into flight modes in multimodal flight control framework and derives the feasible modal sequence based on

Agility Metrics

The development of agility metrics is a research concept motivated by the fact that most of the standard aeronautical performance metrics such as thrust-to-weight ratio and wing loading are not sufficient to describe the transient capabilities of combat aircraft. Traditional metrics tend to measure efficiency or endurance of the aircraft in trimmed flights [45]; however, air combat maneuvering focuses on transitional capabilities of combat aircraft such as turn performance or capturing a specific roll angle. The development and tests of these metrics also play a key role on performance of UCAVs since most UCAVs are expected to have agile maneuvering capability as discussed in the introduction of this article. Agility metrics can be evaluated either from simulations or flight experiments. A collection of such agility metrics can be found in [46] and [47].

Agility metrics are evaluated on different classes and dynamic considerations, such as pitch agility, lateral agility, and axial agility. Some of the popular metrics are displayed in Figures S7 and S8. Figure S7 displays the power loss/onset parameter. Power loss/onset parameter is an axial metric and is an indicator of velocity control capabilities of the aircraft. The second figure is a lateral agility metric called the time-to-capture 90° of roll angle (or TR_{90} in short).

Note that agility metrics depend heavily on the aircraft model and environment conditions. Figures S7 and S8 are obtained from a high fidelity F-16 model described in [37]. Both metrics are plotted against Mach number and angle of attack, which are the primary aerodynamic parameters that influence the variation of the metric.

For practical implementation purposes in Algorithm 1, first a specific agility metric is selected for each mode individually. Later, these metrics are computed offline using numerical simulations of the aircraft model across the specific metric parameter set. From these simulations, angle of attack and modal input pairs, which provide high magnitude agility metrics, are stored in lookup tables. These tables provide the maneuver planner with the ability to select feasible and high performance modal inputs during the planning layer. The selected inputs serve as reference signals to the low level feedback control layer.

Algorithm 1. The generated modal sequence following the solution of the path planner is illustrated in Figure 11, and the timetable of the maneuver sequences is in Table 2.

The extensive treatment of the flight path and maneuver planner algorithm can be found in [41] and [44], which also include a discussion on the real-time performance of the overall architecture.

Agile Maneuver Control Application: Aerobatics Competition Sequence

This second and more control-oriented application considers autonomous control of an aerobatic competition

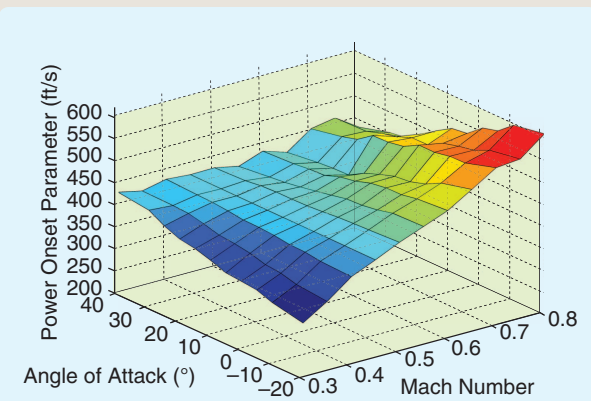


FIGURE S7 Power onset/loss parameter. This metric represents the agility in level-flight mode and provides a preferable region for selecting the velocity (i.e., the modal input of level flight) as well as angle of attack. The figure shows how the velocity should be adjusted to keep the magnitude of agility metric high while keeping the angle of attack fixed.

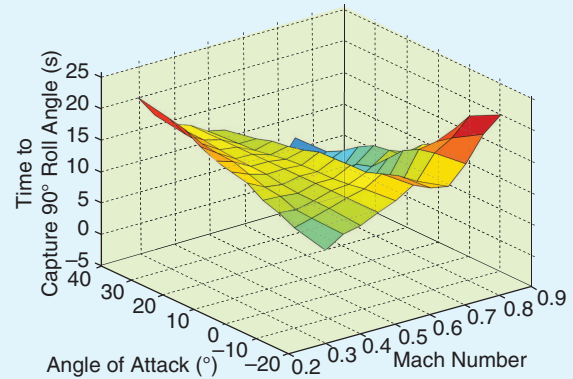


FIGURE S8 Time to capture 90° of roll angle. This metric represents the agility in roll mode and provides a preferable region for selecting the modal input and angle of attack for roll dynamics.

TABLE 2 Modal sequence for the flight plan in the urban environment.

Mode	Label	Time Intervals (s)
q_1	Level flight	[0, 0.83]
q_4	Longitudinal loop	[0.83, 1]
q_2	Dive	[1, 3.57]
q_6	Roll mode	[3.57, 4.57]
q_3	Lateral loop	[4.57, 26.7]
q_5	Pitch yaw transition	[26.7, 27.8]
q_6	Roll mode	[27.8, 29]
q_1	Level flight	[29, 32.3]

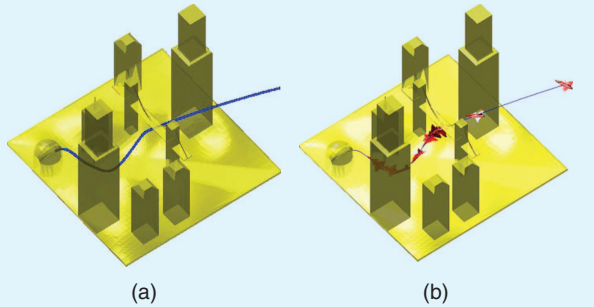


FIGURE 11 Integration and solutions of the path planner and maneuver planner. (a) shows the output of the path planner, and (b) shows the output of the maneuver planner.

sequence inspired from [32]. The overall path of the sequence and the attitude of the aircraft is shown in Figure 12. Here the mode sequence is written in red labels, and the names of the maneuvers from the aerobatics literature are written in black labels. The time history of the velocity is given in Figure 13, while the aerodynamic angles α and β histories are given in Figure 14. The time history of normal acceleration, which is a primary indicator of aggressiveness of the maneuver sequence, is shown in Figure 15. The time history of the body angular rates, along with reference signals generated by low-level controllers, is shown in Figure 16. The input history of the throttle and control surface deflections is shown in

Algorithm 1: Feasible Maneuver Sequence Generation

- 1: INPUT:** Time-parameterized flight path $[n_p(t), e_p(t), h(t)]$, Initial discretization time interval Δt .
 - 2: OUTPUT:** Modal sequence $(q_j^i, m_j^i, \tau_i), i = 1, 2 \dots, N$.
 - 3: Discretize the flight path into M maneuver modes, with duration Δt between each. Approximate the wind-axis Euler angles using (4).
 - 4: Label each mode as level flight, climb/descent, longitudinal loop, and lateral loop based on the wind-axis Euler trajectory.
 - 5: Select a feasible angle of attack and modal input pair from agility metric graphs/tables for each mode.
 - 6: Compute attitude trajectories using (9). Insert attitude transition modes in between other modes to smooth attitude transitions.
 - 7: If a feasible set of modal inputs and/or mode durations are not found, decrease Δt and repeat Steps 3–6.

Figure 17. The analysis of the modal sequence in Figure 12 is represented phase by phase

- » *Phase I, Level Flight and Vertical Loop:* The sequence starts with level-flight mode and evolves into a vertical loop without any attitude transition. While the aircraft draws a full circle in longitudinal plane, the controller precisely tracks the reference pitch rate

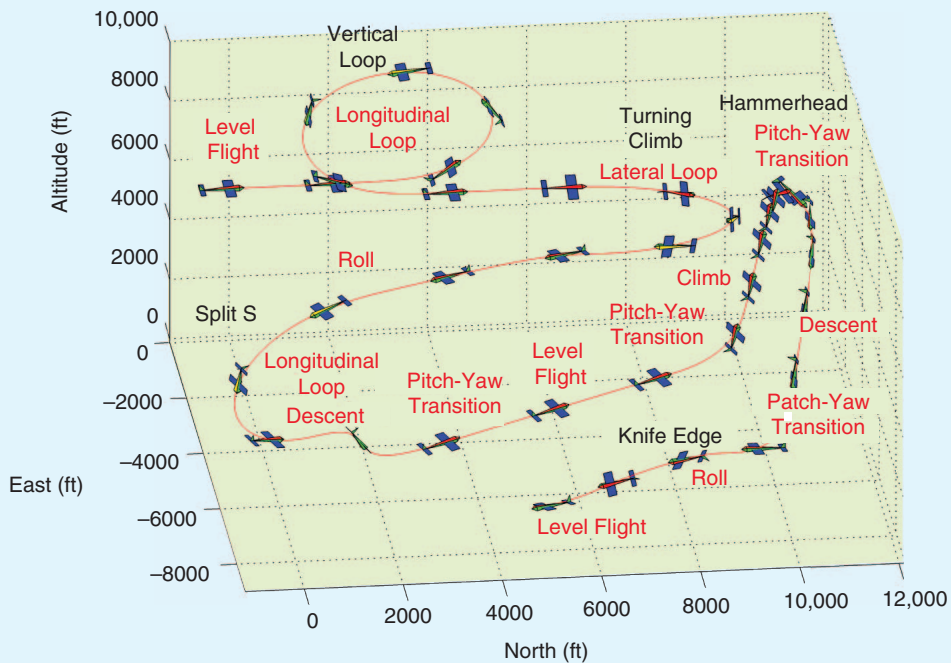


FIGURE 12 Path and attitude history of an aerobatic sequence. The red text refers to maneuver modes, while the black text refers to the names of maneuvers in aerobatics terminology.

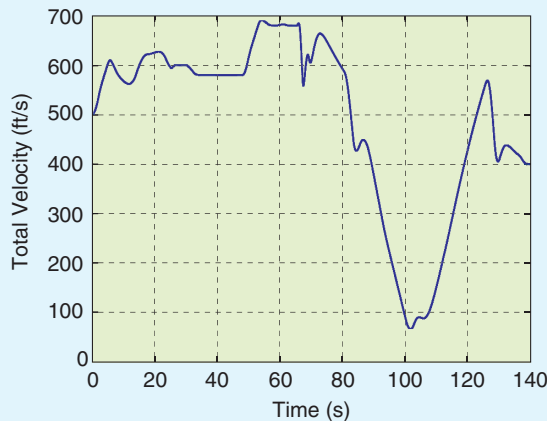


FIGURE 13 Velocity history. The aircraft velocity reaches around 700 ft/s during a loop in split-S and drops down to 100 ft/s during a nearly stalled yaw turn of the hammerhead.

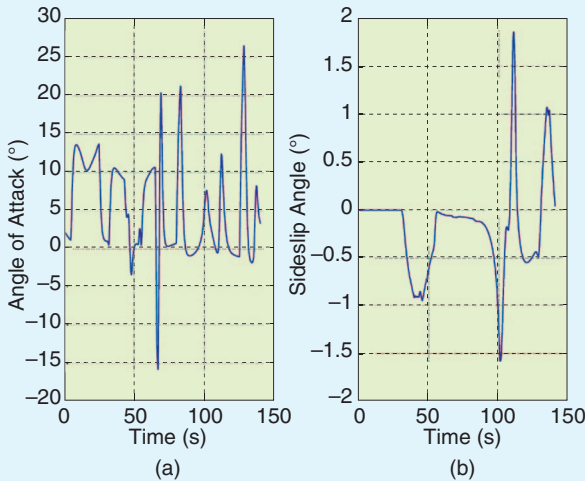


FIGURE 14 Angle of attack and sideslip history. The angle of attack alternates between -20 and 25° during the sequence, which are common values for an aerobatic flight. Note that the sideslip angle is kept nearly at zero during simulation. The constraints placed on every mode is achieved by the controller.

generated by the outer loop, which is a longitudinal loop mode with zero wind-axes yaw angle as a modal input. The aircraft experiences around 6 g during the loop and then regulates back into level-flight mode.

» *Phase II, Turning Climb:* The aircraft enters into a coordinated turning-climbing maneuver, which corresponds to a lateral-loop mode with fixed pitch angle in a multimodal description system. The controller tracks the roll rate and also suppresses the sideslip angle to achieve coordinated flight. By the end of the mode, the aircraft has changed heading by approximately 180° relative to the initial orientation, while continuously climbing.

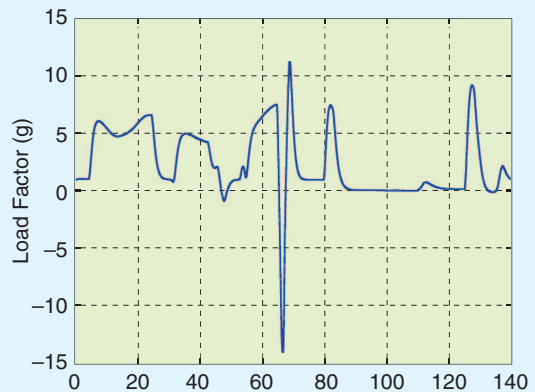


FIGURE 15 Load factor history. It is seen that the load factor alternates sharply between -15 and 10 , which exceeds the g capability of human pilots. This example displays an evident advantage of unmanned combat air vehicles (UCAVs) in battlefield. UCAVs can handle aggressive maneuvers that human pilots cannot handle.

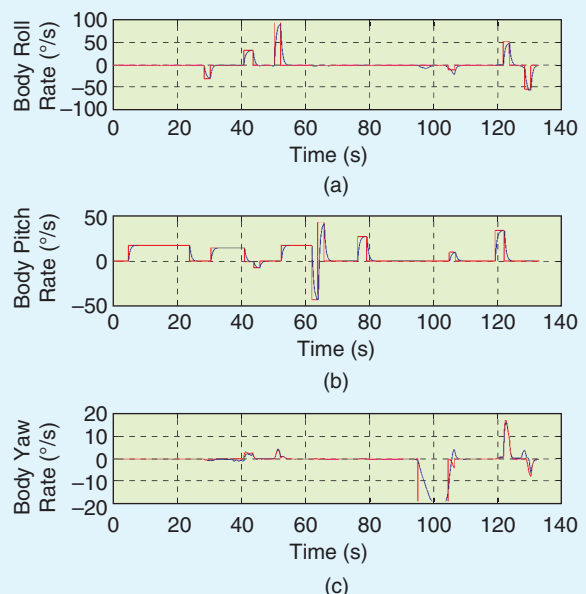


FIGURE 16 Body and reference angular rates history. Reference angular velocities are displayed in red, and actual angular velocities are displayed in blue. The purpose of this plot is to display the performance of the overall switched control system since, in all maneuver modes, angular velocities are tracked at the inner loop. The plot shows that the reference angular velocities are efficiently tracked despite the presence of nonminimum-phase outputs.

» *Phase III, Split-S:* The aircraft reverses its direction by a roll mode to enter into the loop. After completing the half loop, a brief descent followed by level-flight mode is executed. Since these last two modes are incompatible in terms of attitude, a pitch-yaw transition is inserted between these two modes to make a feasible transition between them.

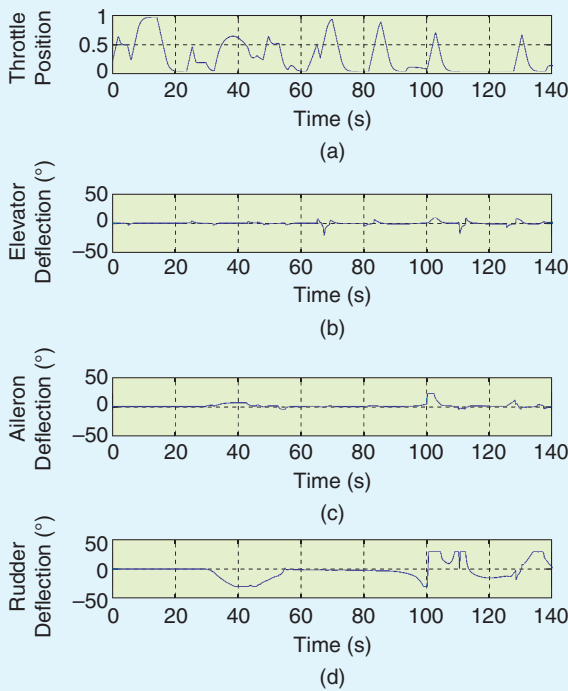


FIGURE 17 Input history. The throttle is switched between full and idle positions during the sequence, similar to what aerobatics pilots do in practice. It is observed that chattering is avoided by the use of a higher order sliding mode.

- » **Phase IV, Hammerhead:** A pitch-yaw transition mode corrects the Euler pitch angle of the aircraft to approximately 90° to make a feasible switch to a sharp climb. While climbing, the aircraft trades speed with altitude, and the speed drops to almost 0 ft/s and the throttle is completely saturated. The aircraft yaws to right and begins to dive while regaining its speed. This maneuver is a popular aerobatics/combat maneuver called a *hammerhead*, which is considered as the highlight of aerobatics competitions.
- » **Phase V, Knife Edge:** The sequence is concluded by a popular aerobatics maneuver known as a knife edge. In this maneuver, the aircraft is banked completely to the right and forced to fly straight in this position; however, this mode can be executed only for a short duration due to loss in lift capacity. The sequence ends with regulation back to level flight.

CONCLUSION

This article treated the planning and control of agile maneuvers, which is a key technology for UCAVs operating in adversary environments. A mode-based maneuvering framework inspired by the modular structure of aerobatics and air combat maneuvers has been presented, and a switching nonlinear control scheme based on sliding mode and higher

order SMC is presented. The overall design is tested both as standalone in autonomous control of an aerobatics competition sequence and as integrated within a flight path planner for navigating in an urban environment.

ACKNOWLEDGMENTS

The authors would like to thank Emre Koyuncu for his insight and contribution to the integration of the framework with a flight path planner and Murat Can Kursun for providing illustrations on aerobatics and air combat maneuvers.

AUTHOR INFORMATION

N. Kemal Ure (ure@mit.edu) received his B.Sc. in aeronautical and astronautical engineering in 2008 and his M.Sc. in defense technologies in 2010, both from Istanbul Technical University. He is currently a Ph.D. candidate and a research assistant at the Aerospace Controls Laboratory at the Massachusetts Institute of Technology. His main research areas are planning and controller design for agile maneuvering aircraft and decentralized planning and learning for multiagent systems. He can be contacted at 77 Massachusetts Avenue, 33-336, Cambridge, Massachusetts 02139 USA.

Gokhan Inalhan is an associate professor at Istanbul Technical University in the Department of Aeronautical Engineering and serves as vice chair of the department and the director of the Controls and Avionics Laboratory. He received his M.Sc. and Ph.D. in aeronautics and astronautics from Stanford University with Ph.D. minor in engineering economic systems and operations research in 1998 and 2004. Between 2004 and 2006, he worked as a postdoctoral associate at the Massachusetts Institute of Technology. During this period he led the Communication and Navigation group in the NASA CER project. He is a member of IEEE Technical Committee on Aerospace Controls and IFAC Technical Committee on Transportation Systems and Aerospace. He serves as a technical expert for the NATO Research Technology Organization, Systems Concepts, and Integration Group.

REFERENCES

- [1] W. Schneider. (2004). Defense science board study on unmanned aerial vehicles and uninhabited combat aerial vehicles, Department of Defense, Tech. Rep. [Online]. Available: <http://www.iwar.org.uk/rma/resources/dsb/uav.pdf>
- [2] J. Gillula, H. Huang, M. P. Vitus, and C. J. Tomlin, "Design of guaranteed safe maneuvers using reachable sets: Autonomous quadrotor aerobatics in theory and practice," in Proc. IEEE Int. Conf. Robotics and Automation, Alaska, May 2010, pp. 1649–1654.
- [3] S. Lupashin, A. Schollig, M. Sherback, and R. D'Andrea, "A simple learning strategy for high-speed quadrocopter multi-flips," in Proc. IEEE Int. Conf. Robotics and Automation, Anchorage, AK, May 2010, pp. 1642–1648.
- [4] R. W. Brockett, "Formal languages for motion description and map making," in Proc. Symp. Applied Mathematics, Louisville, KY, Jan. 16–17, 1990, vol. 25, pp. 180–209.
- [5] J. Lunze and F. Lamnabhi-Lagarrigue, Eds., *Handbook of Hybrid Systems Control*. Cambridge, U.K.: Cambridge Univ. Press, 2009.

- [6] V. Manikonda, P. S. Krishnaprasad, and J. Hendler, "Languages, behaviors, hybrid architectures and motion control," in *Mathematical Control Theory*. J. Baillieul and J.C. Willems, Eds., New York: Springer, 1998, pp. 199–209.
- [7] G. Fainekos, H. K. Gazit, and G. J. Pappas, "Hybrid controllers for path planning: a temporal logic approach," in *Proc. IEEE Conf. Decision and Control*, Seville, Spain, Dec. 10–12, 2002, pp. 4885–4890.
- [8] C. Belta, V. Isler, and G. Pappas, "Discrete abstractions for robot planning and control in polygonal environments," *IEEE Trans. Robot.*, vol. 21, pp. 864–874, 2005.
- [9] C. Tomlin, G. J. Pappas, and S. Sastry, "Conflict resolution for air traffic management: A study in multi-agent hybrid systems," *IEEE Trans. Automat. Contr.*, vol. 43, pp. 509–521, 1998.
- [10] C. Tomlin, J. Lygeros, and S. Sastry, "Controllers for reachability specifications for hybrid systems," *Automatica*, vol. 35, pp. 349–370, 1998.
- [11] R. Ghosh and C. Tomlin, "Nonlinear inverse dynamic control for mode-based flight," in *Proc. AIAA Guidance, Navigation and Control Conf. Exhibit*, 2000, paper no. AIAA-2000-4066, pp. 1–11.
- [12] M. Oishi and C. Tomlin, "Switched nonlinear control of a vstol aircraft," in *Proc. 38th IEEE Conf. Decision and Control*, Phoenix, Dec. 10–12, 1999, vol. 3, pp. 2685–2690.
- [13] E. Frazzoli, M. A. Dahleh, and E. Feron, "Maneuver based motion planning for nonlinear systems with symmetries," *IEEE Trans. Robot. Automat.*, vol. 21, pp. 1077–1091, 2005.
- [14] C. Dever, B. Mettler, E. Feron, J. Popovic, and M. McConley, "Nonlinear trajectory generation for autonomous vehicles via parameterized maneuver classes," *J. Guid. Control Dyn.*, vol. 29, no. 2, pp. 289–302, 2006.
- [15] T. Schouwenaars, J. P. How, and E. Feron, "Receding horizon path planning with implicit safety guarantees," in *Proc. American Control Conf.*, Boston, June 30–July 2, 2004, vol. 6, pp. 5576–5581.
- [16] C. Belta, A. Bicchi, M. Egerstedt, E. Frazzoli, E. Klavins, and G. J. Pappas, "Symbolic planning and control of robot motion," *IEEE Robot. Automat. Mag.*, vol. 14, pp. 61–71, 2007. >
- [17] A. Isidori, *Nonlinear Control Systems*, M. Thoma, Ed. New York: Springer, 1995.
- [18] S. Sastry, *Nonlinear Systems*, J. E. Marsden, L. Sirovich, and S. Wiggins, Eds. New York: Springer, 1999.
- [19] V. I. Utkin, *Sliding Modes in Control and Optimization*. Berlin: Springer, 1992.
- [20] J. J. E. Slotine and W. Li, *Applied Nonlinear Control*. Englewood Cliffs, NJ: Prentice-Hall, 1991.
- [21] S. H. Lane and R. F. Stengel, "Flight control design using nonlinear inverse dynamics," *Automatica*, vol. 24, no. 4, pp. 471–483, 1988.
- [22] M. Azam and S. N. Singh, "Invertibility and trajectory control for nonlinear maneuvers of aircraft," *J. Guid. Control Dyn.*, vol. 17, no. 1, pp. 192–200, 1994.
- [23] E. Frazzoli, M. Dahleh, and E. Feron, "Trajectory tracking control design for autonomous helicopters using a backstepping algorithm," in *Proc. American Control Conf.*, 2000, vol. 6, pp. 4102–4107.
- [24] S. Devasia, D. Chen, and B. Paden, "Nonlinear inversion based output tracking," *IEEE Trans. Automat. Contr.*, vol. 41, pp. 930–942, 1996.
- [25] J. Hauser, S. Sastry, and G. Meyer, "Nonlinear control design for slightly non-minimum phase systems: Application to V/STOL aircraft," *Automatica*, vol. 28, no. 4, pp. 665–679, 1992.
- [26] C. Tomlin, J. Lygeros, L. Benvenuti, and S. Sastry, "Output tracking for a non-minimum phase dynamic CTOL aircraft model," in *Proc. 34th Inst. Electrical and Electronics Engineers Conf. Decision and Control*, New Orleans, Dec. 13–15, 1995, vol. 2, pp. 1867–1872.
- [27] I. A. Shkolnikov and Y. B. Shtessel, "Aircraft nonminimum phase control in dynamic sliding manifolds," *J. Guid. Contr. Dyn.*, vol. 24, no. 3, pp. 566–573, 2001.
- [28] A. Frank, J. McGrew, M. Valenti, D. Levine, and J. How, "Hover, transition, and level flight control design for a single-propeller indoor airplane," in *Proc. AIAA Guidance, Navigation and Control Conf.*, 2007, paper no. AIAA-2007-6318, pp. 1–18.
- [29] V. Gavrilets, A. Shterenberg, M. Dahleh, and E. Feron, "Avionics system for a small unmanned helicopter performing aggressive maneuvers," in *Proc. DASC 19th Digital Avionics Systems Conf.*, 2000, vol. 1, pp. 1E2/1–1E2/7.
- [30] J. Tang, A. Singh, N. Goehausen, and P. Abbeel, "Autonomous helicopter aerobatics through apprenticeship learning," *Int. J. Robot. Res.*, vol. 29, no. 13, pp. 1608–1639, 2010.
- [31] G. Szurovy and M. Gouilan, *Basic Aerobatics*. New York: McGraw-Hill, 1994.
- [32] G. Szurovy and M. Gouilan, *Advanced Aerobatics*. New York: McGraw-Hill, 1997.
- [33] W. K. Kershner, *The Basic Aerobatics Manual*. Ames, IA: Iowa State Univ. Press, 1987.
- [34] R. L. Shaw, *Fighter Combat: Tactics and Maneuvering*. Annapolis, MD: Naval Inst. Press, 1985.
- [35] B. L. Stevens and F. L. Lewis, *Aircraft Simulation and Control*. Hoboken, NJ: Wiley, 2002.
- [36] O. Kato and I. Sugiura, "An interpretation of airplane general motion and control as inverse problem," *J. Guid. Contr. Dyn.*, vol. 9, no. 2, pp. 198–203, 1985.
- [37] L. T. Nguyen, E. M. Ogburn, W. P. Gilbert, K. S. Kibler, P. W. Brown, and P. L. Deal, "Simulator study of stall/post-stall characteristics of a fighter airplane with relaxed longitudinal static stability," NASA, Tech. Rep. 1538, 1979 [Online]. Available: <http://ntrs.nasa.gov>
- [38] O. Kato, "Attitude projection method for analyzing large attitude airplane maneuvers," *J. Guid. Contr. Dyn.*, vol. 13, no. 1, pp. 22–30, 1988.
- [39] Y. Shtessel and I. A. Shkolnikov, "Aeronautical and space vehicle control in dynamic sliding manifolds," *Int. J. Contr.*, vol. 76, no. 9/10, pp. 1000–1017, 2003.
- [40] S. Al-Hiddabi and N. McClamroch, "Tracking and maneuver regulation control for nonlinear nonminimum phase systems: application to flight control," *IEEE Trans. Contr. Syst. Technol.*, vol. 10, no. 6, pp. 780–792, Nov. 2002.
- [41] E. Koyuncu, N. K. Ure, and G. Inalhan, "Integration of path/maneuver planning in complex environments for agile maneuvering UCAVs," *J. Intell. Robot. Syst.*, vol. 57, no. 1–4, pp. 143–170, 2003.
- [42] D. Hsu, R. Kindel, J.-C. Latombe, and S. M. Rock, "Randomized kinodynamic motion planning with moving obstacles," *Int. J. Robot. Res.*, vol. 21, no. 3, pp. 233–256, 2002.
- [43] S. M. LaValle and J. J. Kuffner, Jr., "Randomized kinodynamic planning," *Int. J. Robot. Res.*, vol. 20, no. 5, pp. 378–400, 2001.
- [44] N. K. Ure and G. Inalhan, "Feasible agile maneuver identification and generation algorithms on multi modal control framework," in *Proc. AIAA Conf. Guidance Navigation and Control*, Chicago, IL, Aug. 21–24, 2009, paper no AIAA-2009-5757, pp. 1–18.
- [45] F. J. Hale, *Introduction to Aircraft Performance Selection and Design*. New York: Wiley, 1984.
- [46] J. Valasek and D. R. Downing, "An investigation of fighter aircraft agility," NASA, CA, Tech. Rep. 588, 1993 [Online]. Available: <http://ntrs.nasa.gov>
- [47] R. K. Liefer, "Fighter agility metrics," NASA, CA, Tech. Rep. AD-A22447, 1990 [Online]. Available: <http://ntrs.nasa.gov>
- [48] G. Bartolini, A. Ferrera, and E. Usai, "Output tracking control of uncertain nonlinear second order systems," *Automatica*, vol. 33, no. 12, pp. 2203–2212, 1997.
- [49] A. Levant, "Higher order sliding modes, differentiation and output feedback control," *J. Contr.*, vol. 26, no. 9–10, pp. 924–994, 2003.

